Electronic Theses and Dissertations

2018

Simulation of Non-premixed Ethylene-air Crossflow Jet Flame

Jennifer Onyinye Chikelu
South Dakota State

SIMULATION OF NON-PREMIXED ETHYLENE-AIR CROSSFLOW JET

FLAME

BY

JENNIFER ONYINYE CHIKELU

A thesis submitted in partial fulfillment of the requirements of the

Master of Science

Major in Mechanical Engineering

South Dakota State University

2018

SIMULATION OF NON-PREMIXED ETHYLENE-AIR CROSSFLOW JET FLAME

JENNIFER ONYINYE CHIKELU

This thesis is approved as a creditable and independent investigation by a candidate for the Master of Science in Mechanical Engineering degree and is acceptable for meeting the thesis requirements for this degree. Acceptance of this thesis does not imply that the conclusions reached by the candidate are necessarily the conclusions of the major department.

Jeffrey Doom, Ph.D.   Date

Thesis Advisor

Kurt Bassett, Ph.D.   Date

Head, Department of Mechanical Engineering

Kinchel Doerner, Ph.D.   Date

Dean, Graduate School

ACKNOWLEDGEMENTS

TABLE OF CONTENTS

NOMENCLATURE

u_i, u_j : The velocity component for i and j, m/s

t: Time

σ_{ij} : Sum of Viscous and pressure tensor, N/m^2

τ_{ij} : Viscous tensor, N/m^2

x_i, x_j : Distance in direction i and j, m

ρ: Density of gas, kg/m^3

Y_k : Mass fraction of species k, kg/kg

m: Mass of gas mixture, kg

m$_k$: Mass of species k, kg

W_k : Molecular weight of species k, kg/mole

W: Mean molecular weight of mixture, kg/mole

$V_{k,i}$: Diffusion velocity of species k in direction, i, m/s

$\dot{\omega}_k$, $\dot{\omega}_T$: Mass reaction rate and heat released rate due to combustion respectively

Q_j : Rate of progress of reaction j

$\dot{Q}$: External Heat source term

q_i : Energy flux

$f_{k,i}$, $f_{k,j}$: Volume force acting on species k in direction of i and j.

$\Delta h_{f,k}^0$: Mass formation enthalpy of species k, kJ/kg

E : Sum of sensible and kinetic energy, J

λ : Heat diffusion coefficient

χ : Scalar dissipation rate

D : Diffusion coefficient

K_{fj} , K_{rj} : Forward and reverse rates of reaction j.

A_{fj} : Pre-exponential constant

E_j : Activation energy

T_{aj} : Activation temperature of reaction j, K

β_j : The temperature exponent

R: Gas constant, 8.314J/mole-K

A_s : Total surface area per unit volume of a cloud of monodispersed spherical particle

ρ_{soot} : Density of soot particle

M, N : Soot mass density and soot particle number density respectively.

c_1, c_2, c_3, c_4 : Model constants

k: Turbulent kinetic energy

ϵ : Turbulent Dissipation

μ_t : Turbulence viscosity

P_k: Production of k

P_b : Effect of buoyancy

S, S_{ij}: Mean rate of strain tensor and rate of strain tensor respectively

β : Coefficient of thermal expansion

Pr_t: Turbulent Prandtl number for energy

ν_T : Kinematic eddy viscosity

ω : Specific rate of dissipation.

U_j : Mean Velocity value in j direction

$\alpha, \beta, \beta^*, \sigma, \sigma^*$: Closure coefficients

$C_{1\epsilon}; C_{2\epsilon}; C_\mu; \sigma_k; \sigma_\epsilon$: Model constants

Y_{soot}: Soot mass fraction,

σ_{soot}: Turbulent Prandtl number for soot transport.

$\mathcal{R}_{soot}$: Net rate of soot generation (kg/m^{3}s).

b^*_{nuc}: Normalized radical nuclei concentration (particles $\times$ 10^{-15}/kg).

σ_{nuc} : Turbulent Prandtl number for nuclei transport.

$\mathcal{R}^*_{nuc}$: Normalized net rate of nuclei generation (particles $\times$ 10^{-15}/m^3 -s).

C_a : Coagulation constant.

a: Absorption coefficient.

σ_s: The scattering coefficient.

G: The incident radiation.

C: The linear-anisotropic phase function coefficient.

σ: The Stefan-Boltzmann constant.

S_G : A local radiation source term

I_b: Black body isotropic intensity

I_λ : The local spectral intensity

q_r : The radiative flux

κ_λ : Spectral optical thickness.

η : Wave number.

Ω: Solid angle.

a_η: The spectral absorption coefficient.

I_η: Spectral radiative intensity

β_η: The spectral extinction coefficient

a_η: The spectral absorption coefficient.

$\sigma_{s\eta}$: The spectral scattering coefficient

Φ_η: The scattering phase function

LIST OF FIGURES

LIST OF TABLES

ABSTRACT

SIMULATION OF NON-PREMIXED ETHYLENE-AIR CROSSFLOW JET FLAME

JENNIFER ONYINYE CHIKELU

2018

Computational fluid dynamics tool has been employed in the past to determine and analyze efficiency or performance in combustion engines and for combustion analysis.

This paper represents a systematic investigation on the best model predicts the temperature and soot production in coflow jet flame, by applying various RANS turbulent model, soot models and radiation models in presence or absence of gravity. It also applies this model predicted in crossflow jet flame and investigates the velocity ratio (ratio of the velocity of fuel jet to the velocity of air stream) variation effect on temperature and soot production. ANSYS-Fluent CFD software tool was utilized for this study.

For the co-flow jet result, one-step soot model, SST turbulent model and Rosseland radiation model with gravity was in a reasonable agreement with the Coppalle and Joyeux [50] experimental data that it was compared with. The crossflow jet was simulated with the best model predicted in the coflow, and variation of velocity ratio of fuel jet and air stream was investigated. The results showed that increase in velocity of fuel jet increased temperature and soot volume fraction, which is as a result of an increase in heat released in the reaction zone when fuel concentration increases (velocity of fuel increases) and leading to significant increase in soot production as temperature increases. It was also observed that as the fuel jet velocity/concentration increases, its maximum temperature and soot volume fraction, get further away from the proximity of jet inlet. The effect of mixing of fuel and air streams was also analyzed.

CHAPTER ONE: INTRODUCTION

BACKGROUND

Combustion process has been in our daily life since the beginning of human history. It is an important process to transform chemical energy in fossil or natural fuels into thermal energy which could bring about the mechanical and electrical energy that powers the society. Combustion plays a vital role in automobiles, aircraft, furnaces, power plants and so on. Since combustion process brings about energy source of heat, it is a very crucial and attractive field of study for many reasons. It is necessary to maximize the efficiency of the combustion systems, in order to reduce pollution and maximize profit in the industry.

Combustion process is mostly not environmental-friendly process, since various types of polluted gases can be emitted from the process. Most combustion fuels are composed of simple or complex hydrocarbons, which when oxidized and under combustion reaction, it can bring about emission of soot particles, NOx, SOx, VOC's, CO, CO_2, PAHs, etc. Effects of emissions of these pollutants are as important as energy sustainability in the present society. These pollutants can bring about a vast amount of health problems as well as environmental pollution. Most of these pollutants enhance global warming, and health issues vary from a number of diseases such as lung cancer, heart attack, difficulty in breathing and even death [55]. Strict pollutant emission regulations require a detailed mechanism to predict pollutant species such as NOx, unburned hydrocarbons, and soot [56].

The development of clean energy is very vital, and cannot be overlooked, hence introduces challenges in manufacturing of clean and efficient combustion systems. Researchers try to

design various combustion systems by altering various operating conditions, and turbulent reacting flows are very complex process. The setbacks which make turbulent reacting flows complex are;

1. Complex and large chemical mechanisms, which involves hundreds and thousands of reactions, depending on the type of fuel used, are required to describe the chemical aspect of combustion [1,2]

2. Large computational domains due to turbulence. That is a wide range of length and time scale is usually present in turbulent reacting flows and this increases complexity.

3. Flame radiation heat transfer in internal combustion engines for flame propagation can bring about complexity also [3].

CONSERVATION EQUATIONS FOR REACTING FLOWS.

The conservation equation for reacting flows are somewhat similar to the Navier-stokes equation for non-reacting cases. The difference is because a reacting gas is a non-isothermal mixture of multiple species (hydrocarbons, oxygen, water, etc.), species react chemically and at the rate of reaction differs depending on a specific modeling. Also, since the gas is a mixture of gases, transport coefficients (heat diffusivity, species diffusion, viscosity, etc.) require specific attention [3].

Derivation of these equations presented in equations below may be found in books Williams [4] or Kuo [5].

Mass: $\dfrac{\partial \rho}{\partial t} + \dfrac{\partial \rho u_i}{\partial x_i} = 0$ (1)

Species for k = 1 to N-1 (or N if total mass is not used)

With diffusion velocities:

$$\frac{\partial \rho Y_k}{\partial t} + \frac{\partial}{\partial x_i}\left(\rho\left(u_i + V_{k,i}\right)Y_k\right) = \dot{\omega}_k \tag{2}$$

Momentum:

$$\frac{\partial}{\partial t}\rho u_j + \frac{\partial}{\partial x_i}\rho u_i u_j = -\frac{\partial \rho}{\partial x_j} + \frac{\partial \tau_{ij}}{\partial x_i} + \rho \sum_{k=1}^{N} Y_k f_{k,j} \tag{3}$$

Energy (sum of sensible and kinetic):

$$\frac{\partial \rho E}{\partial t} + \frac{\partial}{\partial x_i}\left(\rho u_i E\right) = \dot{\omega}_T - \frac{\partial q_i}{\partial x_i} + \frac{\partial}{\partial x_j}\left(\sigma_{ij}u_i\right) + \dot{Q} + \rho \sum_{k=1}^{N} Y_k f_{k,i}\left(u_i + V_{k,i}\right) \tag{4}$$

$$with \ \dot{\omega}_T = -\sum_{k=1}^{N} \Delta h_{f,k}^0 \dot{\omega}_k \ and \ q_i = -\lambda \frac{\partial T}{\partial x_i} + \rho \sum_{k=1}^{N} h_k Y_k V_{k,i} \tag{5}$$

The Navier Stokes equation is the basics of mathematical analysis of turbulent reacting flows. This set of equations includes species transport equation with chemical source terms to address chemical transformation, employs absolute enthalpy instead of internal energy as energy variable. Heat release by chemical reaction produces high temperature in the flow field, which leads to variable density effect [3]. The high temperature results in thermal radiation which is important in heat transfer.

TURBULENT NON-PREMIXED FLAMES.

Most combustion applications occur in a turbulent environment. The turbulence and chemical kinetics are a very challenging problem. The strong nonlinear interactions between turbulence and chemistry make combustion hard to understand. Turbulence/chemistry interaction, TCI, was brought about by the fact the mixing processes

in a turbulent flow are not as fast compared with rates of chemical reaction [54]. The time scales of chemical reactions can range from 10^{-10} to more than 1 second [6], while the time scale of turbulent mixing typically is no smaller than 10^{-3}s or 10^{-4} s [7]. The large spatial and temporal variations in species composition and temperature occur in turbulent combustion.

The first description of turbulent combustion is due to Damkohler (1940), which introduced wrinkling as the main mechanism controlling turbulent flames. A turbulent flame speed, S_T, is defined as the velocity needed at the inlet of a control volume V to keep a turbulent flame stationary in the mean inside this volume [3]. One dimensional turbulent flame propagating along x_i, the mean fuel mass fraction balance equation lead to [3]

$$\rho_1 s_T \frac{\partial \check{Y}_F}{\partial x_i} = -\frac{\partial}{\partial x_i}\left(\overline{V_{F,\iota} Y_F} + \bar{\rho}\, \overline{u_i'' \check{Y}_F''}\right) + \bar{\dot{\omega}}_F \qquad (6)$$

In premixed combustion, turbulent mixing creates pockets of cold unreacted and hot reacted mixture, while in non-premixed combustion, the turbulent mixing creates pockets of fuel-rich and fuel-lean mixture [57].

Turbulent non-premixed flames occur in a large number of industrial systems due to they are simpler to build compared to premixed flames, because of perfect mixing of the reactants in a given proportion is not required. They are also safer to operate as they do not exhibit propagation speeds and cannot flashback or autoignite in undesired locations [3].
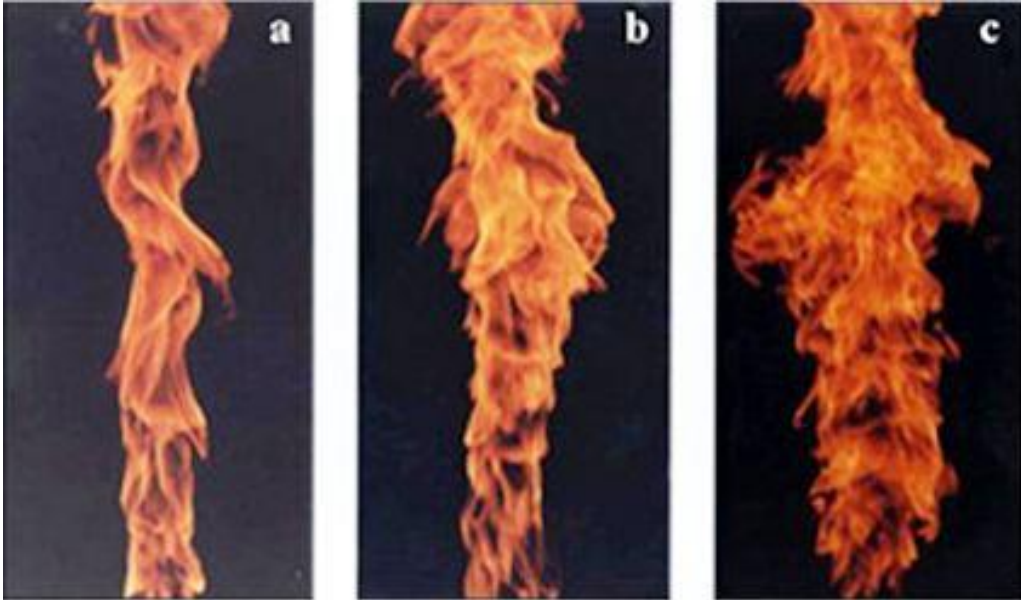
Figure 1: Muniz et al [8] showed images that are short exposure (1/1000 s) soot emission photographs of turbulent ethylene flames at (a) $Re_o = 8,200$, (b) $Re_o = 15,600$ and (c) $Re_o = 24,200$. The axial view extends from 85 to 160 diameters (39 to 73 cm) from the burner exit.

Examples of turbulent non-premixed flames are as follows;

- Conventional gas turbine

- Bi-propellant rocket engines.

- Diesel engines

- Cement kilns, glass furnaces, boiler furnaces.

- Turbojet afterburners.

- Flares in refineries / oil fields.

- Most fires (like forest fires), pool flames.

- Coal/wood combustion.
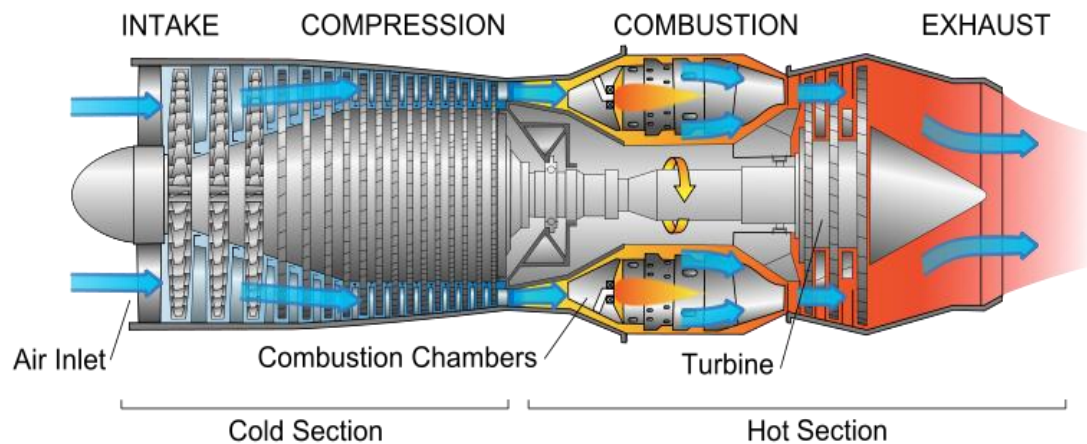
Figure 2 : Diagram of gas turbine jet engine [9].

Non-premixed flames are also called diffusion flames because the reacting species have to reach the flame front before reaction by molecular diffusion. They are exposed to turbulence and diffusion speeds when they travel and can be strongly modified by the turbulence motions. In as much as turbulent premixed flames are safer to operate, some specific processes make it challenging and difficult to for designer to understand. Some of these challenges are [3];

- Combustion intensity and efficiency
- Flame stability.
- Flame shape and size
- Heat transport
- Pollutant emissions.
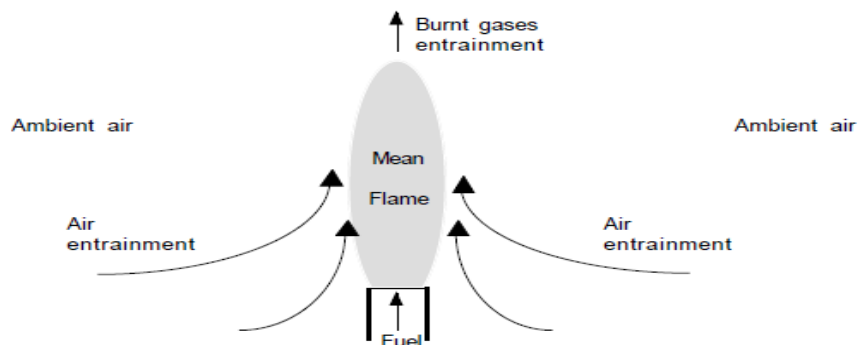
Figure 3 : turbulent non premixed flame. A fuel jet discharges in ambient air. Reaction zone is fed by oxidizer because of air-entrainment. [3]

FLAME STRUCTURE OF DIFFUSION FLAME.

The structure of diffusion flame depends on mixture fraction, z, and on time, t, only. Figure 4 presents a prototype of diffusion flame, fuel and oxidizer diffuse towards the reaction zone where they burn and generate heat, and therefore the temperature is maximum in the reaction zone and diffuses away from the flame front towards fuel and oxidizer stream.
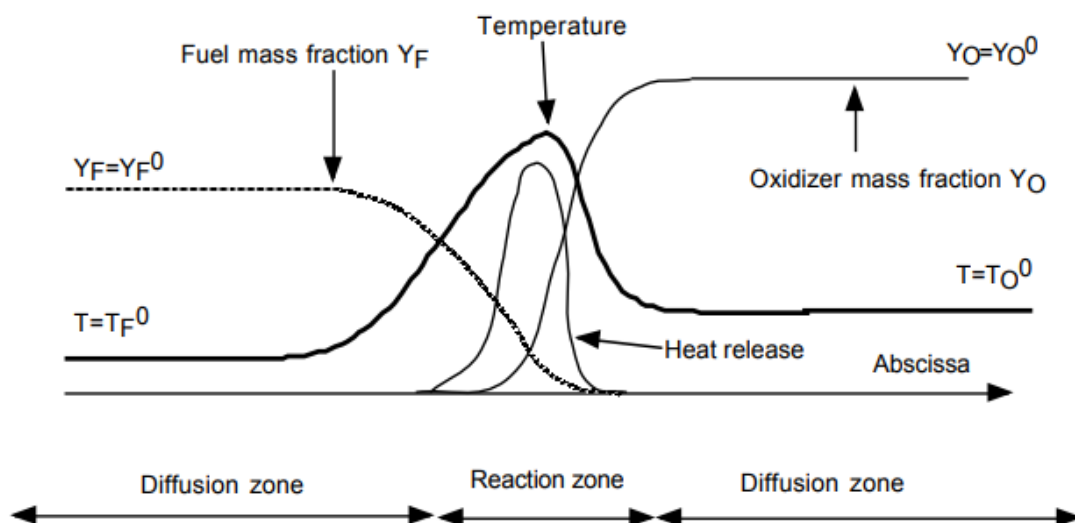
Figure 4: Diffusion flame strucuture [3].

Temperature and species mass fraction which are independent variable, can be written as;

$T = T(z,t) \ and \ Y_k = Y_k(z,t),$

$$Y_k = \frac{m_k}{m} \qquad (7)$$

Where k = species, and Y_k is mass fraction of the species, k. the space, z_j is called mixture fraction of reaction j, and measures fuel/oxidizer ratio. The boundary conditions used was such that $z_j=1$ is in the fuel stream, while $z_j=0$ in the oxidizer stream.

The equation for modelling mass fraction of various species and temperature in time and space, z, is given as ;

$$\rho \frac{\delta Y_k}{\delta t} = \omega_k + \frac{1}{2} \rho\chi \frac{\delta^2 Y_k}{\delta z^2} \qquad (8)$$

$$\rho \frac{\delta T}{\delta t} = \omega_T + \frac{1}{2} \rho\chi \frac{\delta^2 T}{\delta z^2} \qquad (9)$$

Equation 8 and 9 are called flamelet equation [58,59,60].

Where χ is scalar dissipation rate.

$$\chi = 2D \left(\frac{\delta z}{\delta x_i} \frac{\delta z}{\delta x_i} \right) \qquad (10)$$

D is diffusion coefficient. $\chi \ is$ dependent on spatial variable x_i which controls mixing. Once χ is specified, the flamelet equation can be solved in z space to provide flame structure, i.e temperature and species as function of mixture fraction z, and time, t.

Also $\omega_k \ and \ \omega_T$ are mass reaction rates, and heat released due to combustion respectively. They can be derived from;

$$\omega_k = W_k \sum_{j=1}^{M} (v_{kj}) \mathcal{Q}_j \qquad (11)$$

where $\mathcal{Q}_j$ is rate of progress of reacton j.

$$\mathcal{Q}_j = K_{fj} \, \Pi_{K=1}^{N} \left(\frac{\rho Y_k}{W_k}\right)^{v'_{kj}} - K_{rj} \, \Pi_{K=1}^{N} \left(\frac{\rho Y_k}{W_k}\right)^{v''_{kj}} \qquad (12)$$

$$K_{fj} = A_{fj} \, T^{\beta j} \, exp\left(-\frac{E_j}{RT}\right) = A_{fj} \, T^{\beta j} \, exp\left(-\frac{T_{aj}}{T}\right) \qquad (13)$$

$$\omega_T = -\sum_{k=1}^{N} (\Delta h_{f,k}^o) \omega_k \qquad (14)$$

$$\rho = \sum_{k=1}^{N} \rho_k \qquad (15)$$

Mean   Molecular   weight,   W,   of   mixture   given   by

$$\frac{1}{W} = \sum_{k=1}^{N} \frac{Y_k}{W_k} \qquad (16)$$

Flamelet equations/code used for this study was from ANSYS-fluent.

COMPUTATIONAL MODELLING OF TURBULENT COMBUSTION

There various computational models for non-premixed turbulent flames which are the Reynolds averaged Navier Stokes (RANS) model, large eddy simulation (LES) model and Direct numerical simulation (DNS) model.

- Reynolds averaged Navier Stokes (RANS) computation is an easier and first approach because calculating the instantaneous quantity in the flow field in a turbulent flame was impossible[3,12]. Therefore the instantaneous flow field quantities were solved for their mean values. The balance equations for Reynolds or Favre (i.e mass-weighted) averaged quantities are obtained by averaging instantaneous balance equations. The RANS model consisted of turbulence model to deal with flow dynamics in combustion, and a turbulent combustion model to solve chemical species conversion and heat release. The RANS equations provide averaged quantities at an averaged given amount of time for stationary mean flows or for periodic/ cyclic flows like in piston engines. RANS prediction of temperature at a given point in time is constant, which corresponds to mean temperature at that point for a stabilized flame[3]. The RANS equations are derived from equations shown in equation 1 to 4.
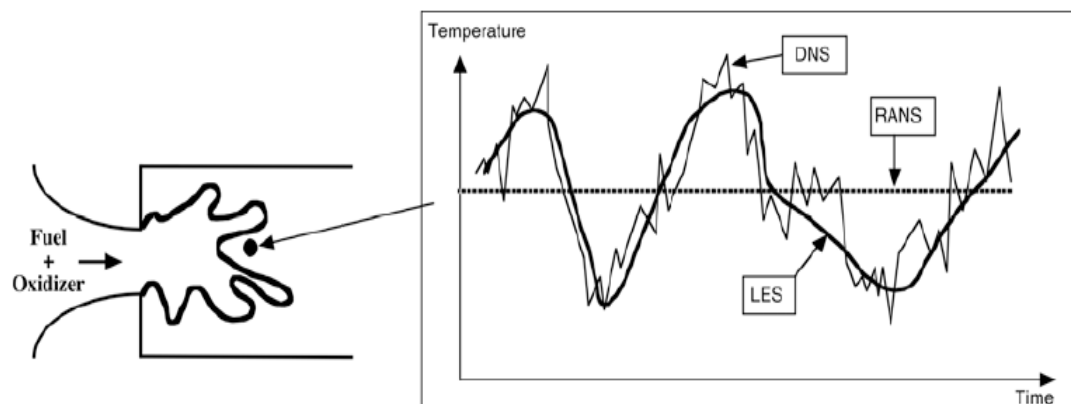
Figure 5: time evolution of local temperature computed with DNS, RANS or LES in a turbulent flame brush.[3].

- Large eddy simulations (LES) are explicitly solved. LES resolves the instantaneous position of a large scale flame front, but a subgrid model would still be required to

determine the effects of small turbulent scales. Therefore LES determines low-frequency variations of temperature as shown in Figure 6. LES model costs more than RANS to run, and 3D simulations are mostly required, while 3D is not required in RANS [3,12].

- Direct numerical simulation DNS is the full instantaneous Navier-Stokes equations are solved explicitly without any model for turbulent motions. DNS predicts all time variations of temperature as in Figure 6, and turbulent small scales are explicitly calculated. No models are needed for turbulence/ combustion interaction. Most DNS models are expensive to run or develop and is limited to academic problems [3].

SOOT FORMATION

Soot consists mostly of carbon. Combustion of hydrocarbons generally produces soot under normal conditions. Combustion of hydrocarbons mainly leads to produce carbon dioxide and water as one of its products. Practically, in fuel-rich regions, the combustion of hydrocarbons produces intermediate species and radicals that lead to the production of soot particles. The soot emitted from long –residence time turbulent non-premixed flames, including toluene, benzene, acetylene, propylene, and propane flames burning in air, have the following elemental mole ratio ranges: C:H of 8.3-18.3, C:O of 58-109, and C-N of 292-976 [17]. Soot particles are very small, ranging in size from 5nm to 80nm, but maybe to several microns in extreme cases [18]. Soot density is less than that of carbon black and in the range of 1700 – 1800 kg/m^3, depending on soot porosity [19]. Soot are mostly spherical in shape but may also appear in agglomerated chunks and even agglomerated filaments [17]. From previous experiments, the soot volume fraction of most diffusion flames ranges from 10^{-6} to 10^{-8} [18].

Soot formation involves highly complicated chemical and physical processes. It can be surprising that hydrocarbon fuel molecules contain very few carbon atoms produces soot particles that contains millions of carbon atoms. Therefore, predicting soot formation is important and its interests are of the following reasons [54];

- Incomplete combustion leads to formation of soot, which reduces combustion efficiency and therefore the engine efficiency.

- Soot /soot particles formed are a major pollutant and have a hazardous effect on human health.

- Although soot formation has its merits, as it enhances heat transfer through radiation in industrial applications such as furnace and heat generators. However, the soot has to be oxidized before they are exhausted into the environment.

- Soot is a vital industrial product known as carbon black. Carbon blacks are used for various applications such as filler in tires, or other materials, toner in copiers, and black pigment in color printings.

Soot formation as stated earlier is a highly sophisticated chemical and physical process, and can be divided into four principal sub-processes which are;

- ➢ Soot particle inception or nucleation.
- ➢ Surface growth.
- ➢ Soot coagulation.
- ➢ Soot oxidation.

Soot Inception

Soot inception or nucleation is the formation of the smallest solid soot particles from gas-phase hydrocarbon molecule of relatively lower molecular weight. This process is a link between the gas-phase combustion zone chemistry and soot particle dynamics [54]. It is one of the determinant factors for the number and mass of the soot particle. There are three major soot inception/nucleation pathway proposed and differ in the key gaseous precursors, and they are acetylene, polyacetylenes, ionic species, or polycyclic aromatic hydrocarbons (PAHs).

PAH pathway involves the formation and growth of aromatic species, where the starting point is formation of first aromatic ring (benzene). These small aliphatics are the building blocks of soot formation, they grow to form large PAHs through HACA (H-abstraction-C_2H_2-addition) mechanism. The HACA mechanism which involves removal of hydrogen atom by a gaseous hydrogen atom, followed by addition of a gaseous acetylene to the radical site formed. In literature, the soot inception rate can be described by the acetylene inception model, the PAH inception model or the naphthalene inception model [20]. Using the acetylene inception route [21,22]. the soot inception rate is given by:

$$\left(\frac{dM}{dt}\right)_{inception} = c_1 M_P \frac{\rho Y_{C2H2}}{W_{C2H2}} e^{-\frac{21100}{T}} \qquad (17)$$

Where M is soot mass density.

Inception also contributes to soot particle number density, N

$$\left(\frac{dN}{dt}\right)_{inception} = \frac{N_A}{M_P}\left(\frac{dM}{dt}\right)_{inception} \qquad (18)$$

M_P is the mass of a soot nucleus and N_A is the Avogadro's number. Model constant c_1 is taken as $54 s^{-1}$ [21]. Y_i and W_i are mass fraction and molecular weight of species I, respectively.

$$M_P = W_C \times N_{soot} \qquad (19)$$

Where Wc is the molecular weight of carbon atoms and N_{soot} represents the number of carbon atoms in one soot nucleus.

Soot inception model based on PAHs such as naphthalene and phenanthrene was proposed by Hall et al. (1997) [23].

$$\left(\frac{dM}{dt}\right)_{inception} = c_2\rho^2 \frac{(Y_{C2H2})^2 Y_{C6H5}}{Y_{H2}} e^{-\frac{4378}{T}} + c_3\rho^2 \frac{Y_{C2H2}Y_{C6H6}Y_{C6H5}}{Y_{H2}} e^{-\frac{6390}{T}} \qquad (20)$$

Where model constants $c_2 \ and \ c_3 \ are \ 3.70 \times 10^6 \ and \ 7.21 \times 10^6$, respectively. The first term in equation 12 corresponds to formation of naphthalene ($C_{10}H_8$), and the second term corresponds to formation of phenanthrene. The second term is negligible in ethylene/air non-premixed flames [20]

Soot Surface Growth

Addition of gas-phase material to an already formed particle is the surface growth. Surface growth leads to mass accumulation of soot particles. As explained at inception, surface growth occurs through the HACA mechanism, where acetylene reacts with particle surface, although PAHs may also play a role. Factors that determine surface growth are the available surface area and the number of active sites on the surface. The surface growth

decreases with time or with the extent of particle growth, because of the decrease of active sites and available surface area for HACA mechanism. This is called "surface aging" [54].

The number of active sites is assumed to be proportional to the surface area of particles, where total surface area per unit volume of a cloud of monodispersed spherical particle is

$$A_s = (\pi N)^{\frac{1}{3}} \left(\frac{6M}{\rho_{soot}} \right)^{\frac{2}{3}} \qquad (21)$$

The surface growth term can be written as;

$$\left(\frac{dM}{dt} \right)_{growth} = c_4 \rho \frac{Y_{C2H2}}{W_{C2H2}} e^{-\frac{T_a}{T}} f(A_s) \qquad (22)$$

Where c_4 is a model constant, T_a is activation temperature, ρ_{soot} is the soot density (1800 kg/m³). $f(A_s)$ can be equal to A_s or $\sqrt{A_s}$ or N.

Soot Coagulation

Soot coagulation is more of a physical process, where collisions between these particles lead to the formation of larger soot particles. Soot coagulation occurs simultaneously with soot growth, the difference is while soot growth affects the mass of soot particles, soot coagulation only affects the number density, N, by the changes in the evolution of the soot particle size distribution. Particle coagulation is classified into two processes which are coalescent collision and agglomeration. The coalescent collision, two particles come together and merge to form one larger particle, while in agglomeration, two particles come together to form chain-like structure but the identity of each particle is maintained. Agglomeration may start at the onset of soot inception [54].

The Smoluchowski equation assumed the particles are monodispersed in size and spherical, the coagulation rate is expressed as [24];

$$\left(\frac{dN}{dt}\right)_{Coagulation} = -C_a \cdot \left(\frac{24R_g}{\rho_{soot}N_A}\right)^{\frac{1}{2}} \left(\frac{6}{\pi\rho_{soot}}\right)^{\frac{1}{6}} T^{1/2} M^{1/6} N^{11/6} \qquad (23)$$

Where R_g is the universal gas constant and C_a is the coagulation constant.

Soot Oxidation

Oxidation is the destruction of soot by changing the mass of solid soot particle into gas phase species. This process removes carbon from the surface of soot particle using oxidizing agents before they are released or exhausted [25]. The main oxidizing agents for soot particles are hydroxyl radical (OH) and oxygen molecule. The oxidation process brings about reduction in mass of soot particle, therefore the rate of soot mass consumption is defined as;

$$\left(\frac{dM}{dt}\right)_{Oxidation} = -\sum w_i \, (\pi N)^{\frac{1}{3}} \left(\frac{6M}{\rho_{soot}}\right)^{2/3} \qquad (24)$$

Where w_i (kg.m^{-2}s^{-1}) is the specific surface oxidation rate [25].

RADIATION MODELLING

Radiation heat transfer is very important in the combustion process since the rate of radiative heat transfer depends on temperature to the fourth power or higher. Thermal radiation is also important especially when soot particles are present, and exerts effects at a distance. It also allows energy to travel directly from hot to cold regions such as reactant mixtures and the surrounding. Thermal radiation in flames has complicated calculations.

Its integral equation containing up to seven independent variables which are the frequency of radiation, three space coordinates, two coordinates describing the direction of radiation and time. Inadequate radiation calculations can cause large errors in determining the flame structure and pollutant emission. Some emissions such as NOx are sensitive to flame temperature distribution, which can affect radiation model [54]. Since temperature is highly coupled with radiation, errors in temperature predictions will over or under-predict soot formation and oxidation rates, and therefore leads to an error in soot yields. The divergence of radiative heat flux, $\vec{q}_R$,

$$\nabla . \vec{q}_R = \int_0^\infty a_\eta \left(4\pi I_{b\eta} - \int_{4\pi} I_\eta \, d\Omega \right) d\eta \qquad (25)$$

Where η stands for wave number, Ω is solid angle, a_η is the spectral absorption coefficient, and I_η is spectral radiative intensity. The subscript b denotes a blackbody property. The absorption coefficient is determined from radiative properties of both gas-phase species and particulates. The radiative intensity is determined from the solution of the radiative transfer equation (RTE) [18].

The RTE describes the radiative intensity field within an enclosure containing a participating medium as a function of spatial location, direction and spectral variable (wavenumber). The participating medium such as flame, experience radiative energy which includes absorption, emission, and scattering, and these can lead to change in intensity of radiation. The RTE can be expressed as [18]:

$$\frac{dI_\eta}{ds} = \hat{s}.\nabla I_\eta = a_\eta I_{b\eta} - \beta_\eta I_\eta + \frac{\sigma_{s\eta}}{4\pi} \int_{4\pi} I_\eta(\hat{s}_\iota) \, \Phi_\eta (\hat{s}_\iota , \hat{s})d\Omega_i \qquad (26)$$

β_η is the spectral extinction coefficient, this is the sum of the spectral absorption coefficient a_η and the spectral scattering coefficient $\sigma_{s\eta}$. The quantity $\Phi_\eta(\widehat{s_\iota}, \hat{s})$ is the scattering phase function and describes the probability that a ray from a certain direction, $\widehat{s_\iota}$ is scattered into a certain other direction, $\hat{s}$.

Methods that have been mostly used in combustion simulations fall into one of the five groups: (1) optically thin approximations; (2) spherical harmonic methods; (3) discrete ordinate methods; (4) zonal methods; and (5) statistical methods. For this study, the spherical harmonic methods are used for radiation modeling.

The spherical harmonic method is also known as the P_N method or differential method. This method expresses the radiative intensity, in the radiative transfer equation (RTE), as a series of products of angular (directional) and spatial functions. P_1 method in FLUENT used in this study is a spherical harmonic method.

CHAPTER TWO: LITERATURE REVIEW

Researchers over the years have analyzed similar studies, and their contributions to the improvement and understanding of soot emissions and temperature in a turbulent non-premixed jet flame are emphasized. Knowledge from previous research work is studied, for the purpose of gaining more understanding on the top, and solving potential problems or questions not answered by literature available.

Lignell et al [33] conducted a computational study on three-dimensional direct numerical simulation of soot formation and transport, which consists of a temporally evolving non-premixed ethylene jet flame. The study employed a four-step, three moment, semiempirical soot model, and a reduced ethylene combustion mechanism. The fuel domain center is surrounded by counterflow oxidizer, the fuel composition was ethylene (0.2546) and nitrogen gas (0.7454), while the oxidizer composition was oxygen (0.2641) and nitrogen (0.7359). The model showed that enhanced turbulent mixing of fuel and oxidizer stream had an effect on the transport of soot particles towards the flame zone. The motion of soot arises from differential diffusion between soot and mixture fraction, as well as the bulk effect of mixing of fuel jet core. It has been previously shown that the location of soot in mixture fraction coordinate has a direct impact on temperature and gas composition of the soot, and hence its radiative heat transfer and reaction rates [33,45].

Hewson et al [34] conducted a study to determine gas temperature, soot concentration and radiative losses, by comparing the one dimensional turbulent Direct numerical simulation model (ODT) and experimental study using measurements such as the femtosecond/picosecond coherent anti-stokes scattering, CARS, scheme [35], for ethylene

jet diffusion flames. The resultant temperatures from both methods were very close. The simulation was also conducted with soot nucleation and growth rates divided by factors of 1, 2, 4 and 8. The varied soot-production rate resulted in a significant difference in the soot mass fraction, the enthalpy and the soot emissions. The case with soot rates divided by 8, was in good agreement with the experimental results on the temperature and average soot volume fraction, which is important for determining soot emissions.

Krishna et al [36] carried out a computational study using CHEMKIN on effects of oxygen-enrichment and fuel unsaturation on flame structure, PAHs, soot and NOx emissions in counterflow flames burning ethylene, propane, and propene. Stoichiometric mixture and fraction of fuel and oxidant are varied and changes in flame structure, PAHs and soot emissions was determined for various fuels. It was discovered that as stoichiometric mixture fraction is increased, the PAHs and acetylene formation is reduced, and with additional soot oxidation, can lead to a non-sooting flame. The reduced soot and PAH formation are as a result of hydrodynamic and flame structure effects. An increase in stoichiometric mixture fraction (higher oxidation) enhances O, OH, and H radical, which reacts with intermediate species to reduce them to smaller hydrocarbons, decreasing soot and PAH formation. Propene and ethylene fuel flames produced more soot than propane fuels because of the double bond present in them.

Hwang and Chung [37] analyzed counterflow diffusion flames of ethylene experimentally and numerically for soot particle growth rate. Classifying diffusion flame into soot formation/oxidation flame (SFO) and soot formation flame (SF). The SFO flames are flames located on the fuel side where soot particles are transported to high temperature oxidizer side and are oxidized. SF flames are when flames are located at the oxidizer side

of a stagnation plane when soot particles are transported towards the stagnation plane, no oxidation occurs, can cause an increase in soot concentration. The study considered soot growth for SFO and SF flames by addition of acetylene to the surface of soot particles (HACA mechanism), and by coagulation of PAHs. The study showed the importance of hydrocarbon radicals other than H is needed for soot surface activation in SF flames, before addition of acetylene. The SFO flames, its soot growth region has high temperature and PAH concentrations are relatively low, whereas for SF flames, its temperatures are low, and PAH concentrations are about 10 times higher than that of SFO flames [37].

Lorenzo et al [38] did a computational study on modeling soot formation and thermal radiation for turbulent diffusion flame using n-Decane (in stoichiometric ratio with toluene) as fuel and air as oxidize. The turbulent model exploited RANS turbulent model which was the k-epsilon and the soot model used was Moss-Brookes-hall and method of moments, and his radiation model was the discrete ordinate method, the simulation was carried out in ANSYS Fluent. He found out Moss-Brookes method was a better model to predict soot formation compared to the method of moments (MoM). He validated his results using experimental results from Young et al (1994) [39].

Ma et al [20] study focused on developing optimal soot model. The study used k-epsilon (RANS) model as the turbulent model, and a diffusion model for an optically thick medium as its radiation model. The soot model source terms, inception, surface growth, coagulation, and oxidation were investigated individually. For the inception term, by comparing the acetylene, PAH, and naphthalene inception route, that of naphthalene performed better. Although from the result shown the soot volume fraction of the acetylene route is closer to the experimental data when Brookes and Moss(1999) [21] surface growth rate model was

used, while naphthalene route was closer to the experimental data when Smooke et al (1999)[40] surface growth rate model was used. The results were validated using Young and Moss's (1994)[39,44] experimental measurements. The surface growth rate is assumed to be proportional to the square root of the surface area.

Gopalendu et al [41] studied the accuracy and computational cost of radiation models in simulating a methane-air non-premixed turbulent jet flame. The radiation models involved had various k-distribution spectral models and RTE solvers, the models compared were the P-1, P-3, finite volume method (FVM), discrete ordinate method (DOM), and line-by-line (LBL) accurate Photon Monte Carlo (PMC) methods with and without considerations of turbulent-radiation interactions(TRI). From the study P-1 model was least expensive, it performed better for optically thinner flames than optically thicker flames. All radiation models gave an accurate prediction for optically thinner flames. The optically thicker flames were predicted accurately by FVM and P-3 with advanced k-distribution methods. The FVM was most expensive though it predicts accurate results for both thick and thin flames.

Wang et al [42, 43] studied oxygen-enriched turbulent non-premixed flames, to find out their interactions with soot, thermal radiation, and NOx emissions. The propane-air coflow configuration, a standard k-ϵ model and a soot model that includes soot formation and oxidation description, and method of moments to describe the evolution of soot particle size distribution was employed. For the two radiation models implemented, one accounts for nongray-gas properties and the other one does not, both radiation models include self-absorption effects and treat soot radiation as gray. The results show: 1) Soot prediction is very sensitive to soot surface growth model and soot formation is closely coupled with

flame temperature through soot radiation, 2) Presence of soot changes flame shape, 3) Soot is distributed in the fuel–rich regions upstream of the nominal flame zone, and 4) Soot radiation decreases flame temperature and *NOx* emissions and effects of non–gray gas phase is important even in the presence of strong gray soot radiation.

Doom and Oefelein (2010) [46] conducted a large eddy simulation of ethylene-air diffusion flame. The study implemented a P-1 gray and nongrey radiation model, and the soot model employed, which accounts for nucleation, growth, coagulation, and oxidation was from Leung et al [47]. Another soot model implemented was a Eulerian-Lagrangian soot model using moment-based model for soot formation and oxidation. They developed their model and validated the simulation using results from CHEMKIN, premixed and diffusion experiments. Soot models were validated using results from Appel et al [48] for premixed flame, and Wang et al (1996) [49] for diffusion flame. Also, an experiment was conducted and soot volume fraction was measured using the Laser Induced Incandescence (LII), and its value was compared to the LES performed. Its results were very close. It showed the model gave a good prediction of soot concentration.

Coppalle and Joyeux [50] experimental results was one of the key validations used in this study. They conducted an experiment to measure the temperature and soot volume fraction in sooting flame in a turbulent diffusion ethylene jet flame. The correlation between temperature and soot volume fraction fluctuation in the three flames which has different buoyancy effects was determined. The study showed the influence of mixing on soot formation in turbulent flames. Just as Wang et al discovered, soot formation influences soot radiation which is coupled with flame temperature. Therefore the three flames also exhibited different flame temperature characteristics.

This study will have almost similar model and objective Santu and Doom [51] study. Their study showed the effect of turbulence model, gravity, soot model and radiation on an ethylene-air coflow diffusion jet flame. They simulated non-premixed flame at Reynold number of 5700. They used various RANS turbulent model, and three soot models which were one step, two step, and Moss-Brookes methods. Also, Rosseland radiation model and no radiation was performed, The results were compared to Coppalle and Joyeux [50] experimental result. The simulation showed that the SST turbulence model, one step soot model and Rosseland radiation model including gravity agrees well with the experimental data for temperature and soot. The flamelet soot modeling (Carbonell et al[53]) and flamelet radiation modeling (Doom [52]) has been incorporated and compared to as well

RESEARCH OBJECTIVES

- This research is geared towards determining the best soot, RANS turbulence and radiation model to predict temperature and soot concentration for non-premixed flame for ethylene-air coflow and validating the results obtained with Coppalle and Joyeux experimental results and Santu and Doom simulations for their coflow ethylene diffusion flame results.

- The best model will be tested on non-premixed flame for ethylene-air crossflow, and varying the velocity of the fuel jet and velocity of crossflow. The velocity ratios are 0.5, 1, 3, 6.3 and 10.

- The effect of turbulence, soot production and radiation are analyzed based on various velocity ratio of the crossflow jet flame.

CONTRIBUTION

➢ Validate model for coflow non-premixed combustion and using the best model on the cross-flow non-premixed combustion for ethylene jet flame.

➢ To determine the effect of various soot model, RANS turbulence model and radiation model on temperature and soot production for the coflow jet.

➢ To determine the effect of variation in velocity ratio of the fuel jet and air crossflow on the soot production and temperature in crossflow jet flame.

➢ Determining the influence of mixing on soot formation and temperature in counterflow diffusion combustion.

CHAPTER THREE: METHOD AND APPROACH

Methods and techniques used in the modeling and simulation of the ethylene air crossflow in ANSYS Fluent and analysis are discussed in this chapter.

Methodology

- Problem statement and initial conditions.

- CAD model generation.

- Discretization.

- Turbulence, Soot and Radiation Models used.

PROBLEM STATEMENT.

- A non-premixed flame of ethylene as fuel entering a defined space in coflow to the oxidizer (air), at an initial temperature of 300K. Ethylene gas having a stoichiometric ratio of 1, and oxygen in air having a mole fraction of 0.21.

- A non-premixed flame of ethylene as fuel entering a defined space in counterflow to the oxidizer (air), at an initial temperature of 300K. Ethylene gas having a stoichiometric ratio of 1, and oxygen in air having a mole fraction of 0.21.

INITIAL CONDITIONS.

For the coflow initial conditions

- The models for non-premixed ethylene coflow jet, where the mean flow of oxidizer is one dimensional in co-stream or similar direction and initial pressure of 1 atm.

- The fuel enters via diameter, D of 9mm, at 6.3m/s, Reynolds number of 5700 at an initial temperature of 300 K.

- The oxidizer stream composition has mole fraction of nitrogen gas and oxygen gas as 0.79 and 0.21 respectively. The oxidizer has an inlet velocity of 1 m/s, this implies velocity ratio of fuel jet and air inlet is 6.3.

For the crossflow initial conditions

- The models for non-premixed ethylene crossflow jet, where the mean flow of oxidizer is one dimensional in cross-stream direction and initial pressure of 1 atm.

- The fuel enters via diameter, D of 9mm and initial temperature of 300 K. The velocity of the fuel jet and velocity of crossflow are varied. The velocity ratios used for the study are 0.5, 1, 6.3 and 10.

- The oxidizer stream composition has mole fraction of nitrogen gas and oxygen gas as 0.79 and 0.21 respectively.

CAD MODEL GENERATION.

For coflow CAD model

The CAD model was generated using the StarCCM+ software. The computational domain is cylindrical with a diameter of 0.54 m and a height of 1.35 m. The fuel inlet diameter is 9 mm. Figure 6 shows the surface parts of the CAD model. The boundary conditions used were fuel inlet and coflow (air inlet) are velocity inlets, the outlet is a pressure outlet, and the pipe is a symmetry plane.

Figure 6: Image showing 3D CAD MODEL for Coflow simulation.

For crossflow CAD model

The CAD model was generated using StarCCM+ software. The size of the computational domain has the length of 1.4 m, in which 1.35 m is the domain where the fuel inlet direction occurs, a height of 0.3 m, and a thickness of 0.135 m. The fuel inlet diameter is 9 mm. Figure 7 shows the surface parts of the CAD model. The boundary conditions used were fuel inlet and inlet (air inlet) are veloci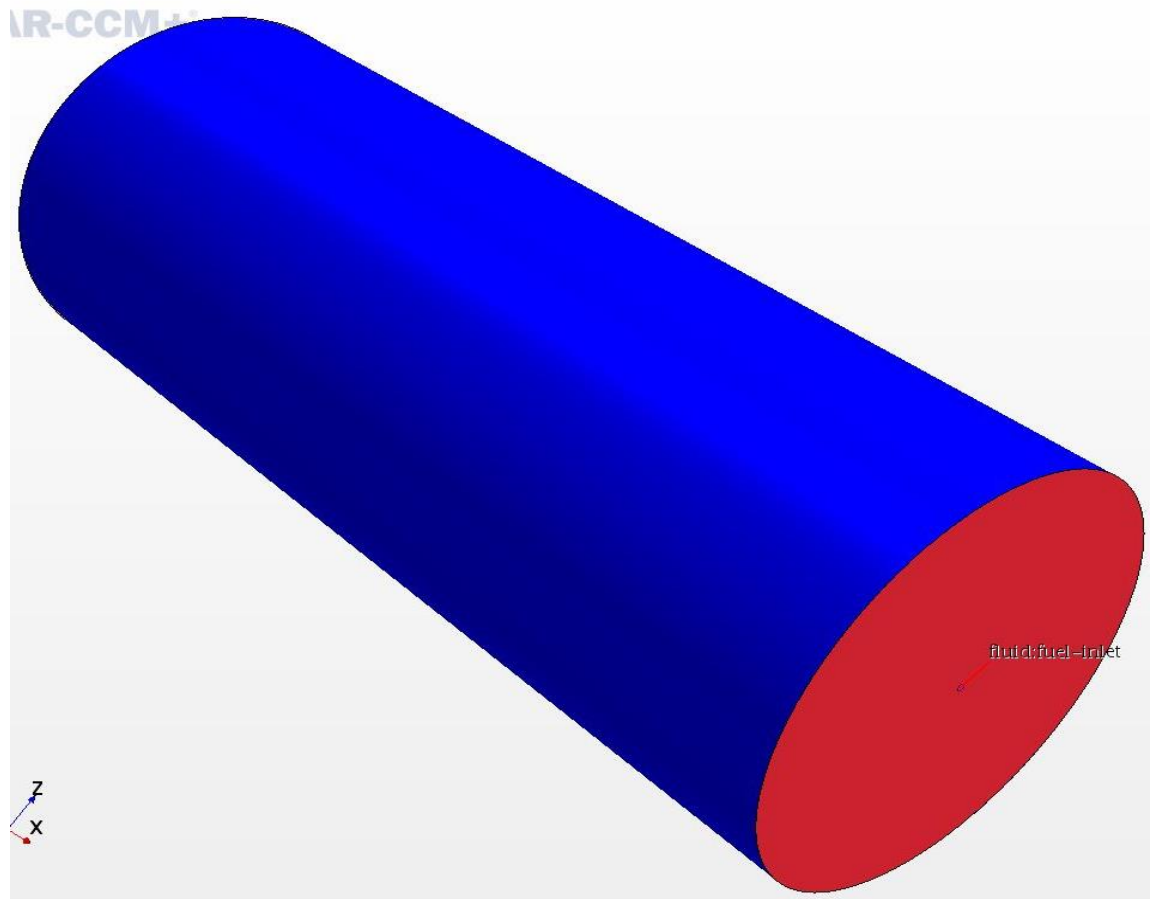ty inlets, the outlet is a pressure outlet, and the other parts such as left, right, top and bottom regions are symmetry planes.
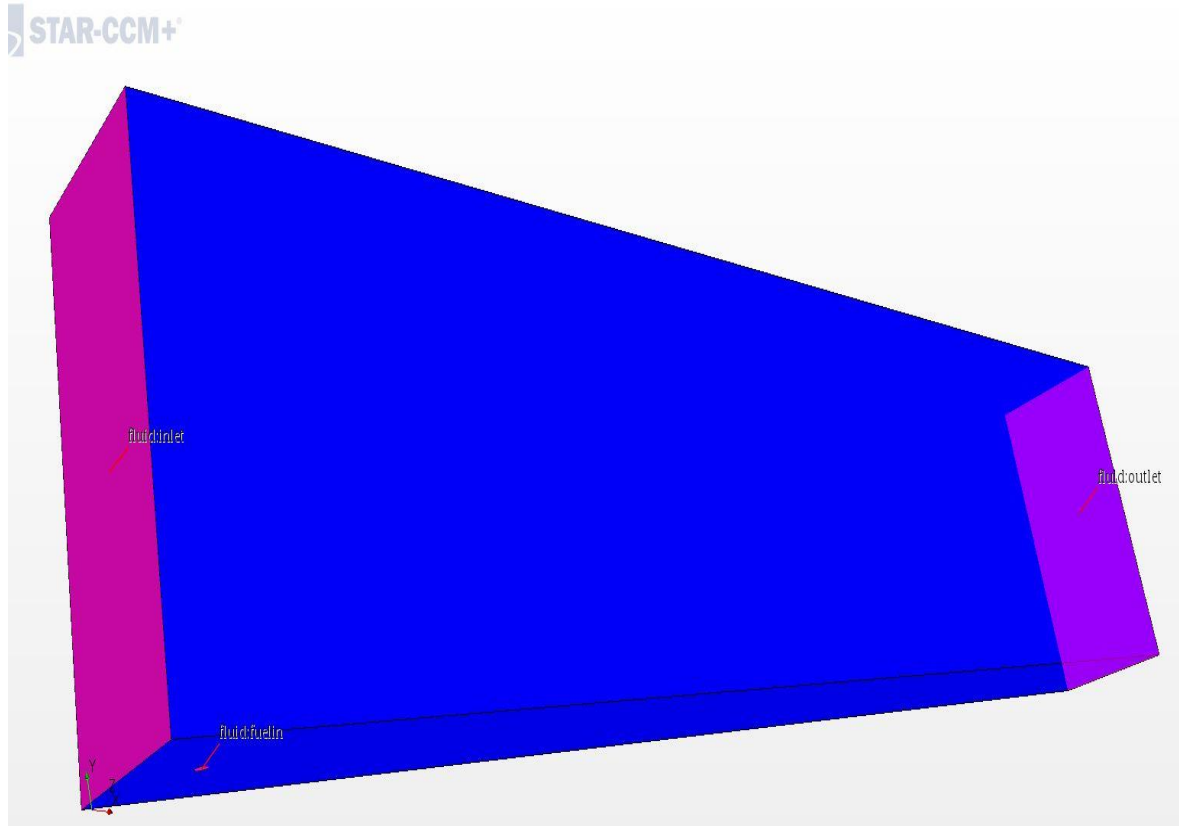
Figure 7: Image showing 3D CAD model for crossflow simulation.

DISCRETIZATION.

The CAD model is discretized using by meshing. In meshing, the regions are divided into smaller areas to enable solvers to give more accurate results. These smaller regions may be in different shapes such as polyhedrons, hexahedrons, tetrahedrons in the case of 3D geometry. The governing equations are discretized over the mesh.

Meshing models used for the simulation for the coflow model;

- Extruder

- Embedded thin mesher

- Polyhedral mesher

- Surface remesher

- Surface wrapper.

- Generalized cylinder

The base size of the mesh used was 9.2 mm, and fuel inlet base size of 0.46 mm. It has 499,331 mixed computational grid cells. The quality of the mesh determined by a maximum aspect ratio of 12.4 and minimum orthogonal quality of 0.635 (which shows a good mesh since is close to 1).

Meshing models used for the simulation for crossflow model;

- Extruder
- Embedded thin mesher
- Polyhedral mesher
- Prism layer mesher
- Surface remesher
- Surface wrapper.

The base size of the mesh used was 4. 7mm, and fuel inlet base size of 0.47 mm. It has 499,173 mixed computational grid cells. The quality of the mesh determined by a maximum aspect ratio of 10.41 and minimum orthogonal quality of 0.67 (which shows a good mesh since is close to 1).

Figure 8: Meshing image for coflow CAD model with target base size of 9.2 mm and

Coflow CAD detailed mesh of the fuel inlet with target base size of 0.46 mm

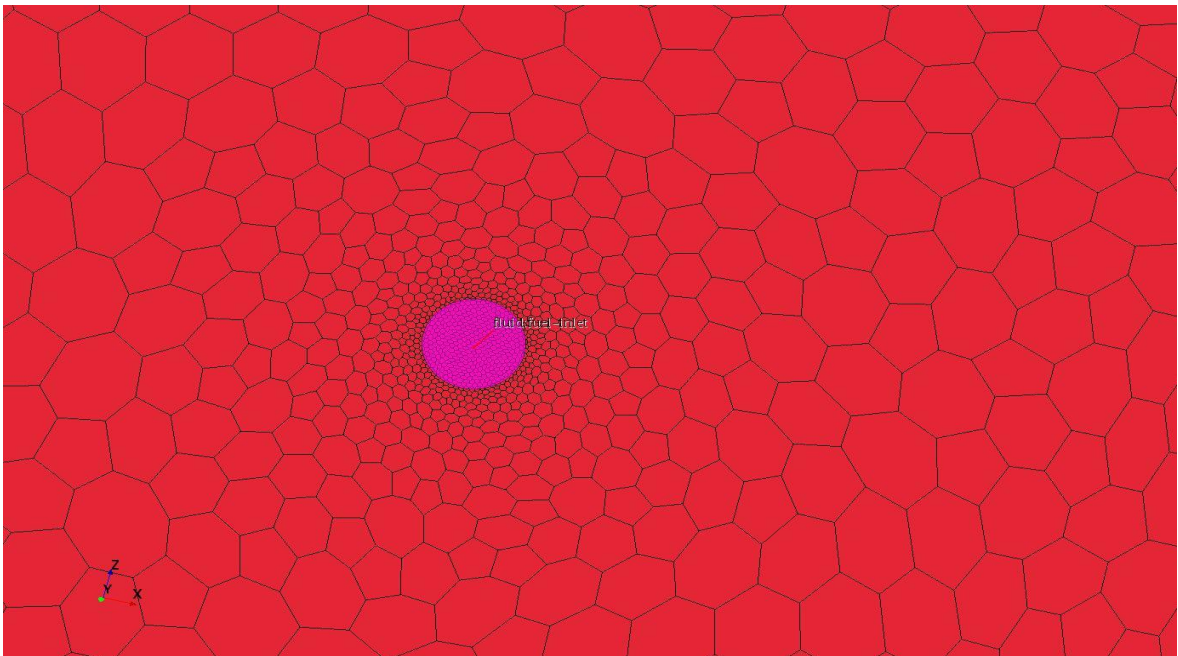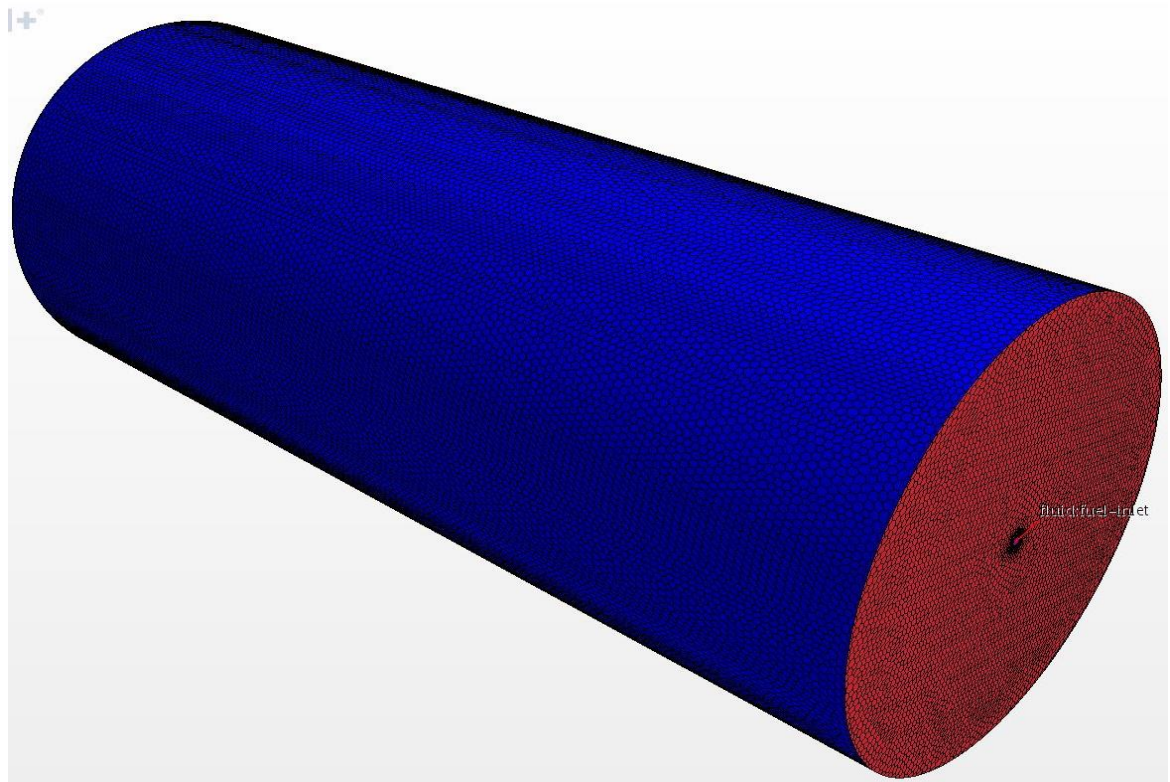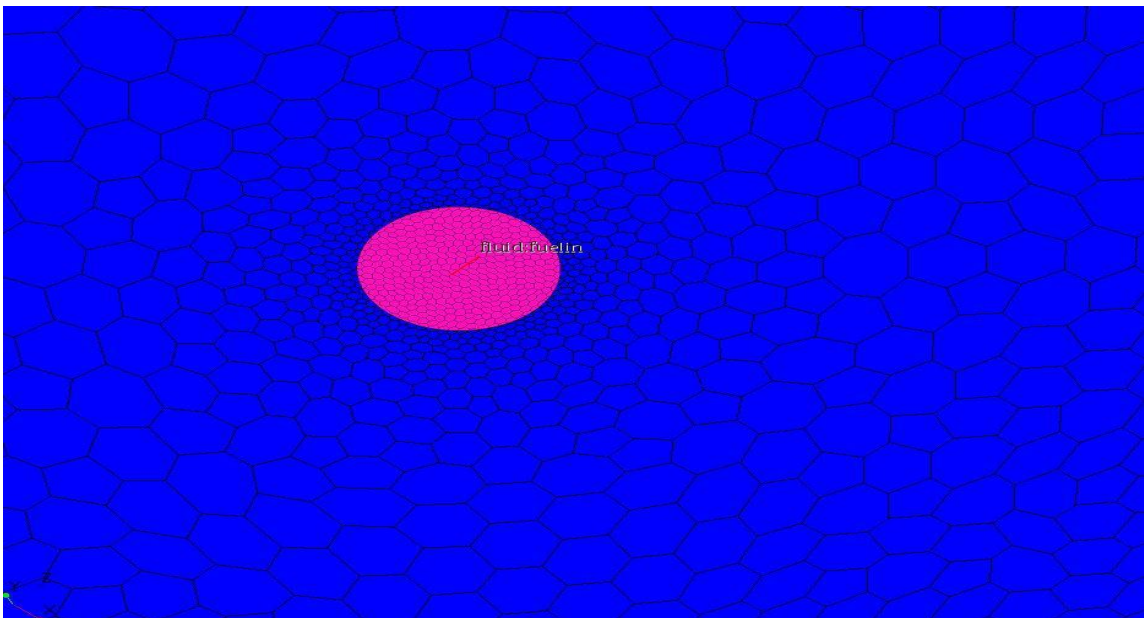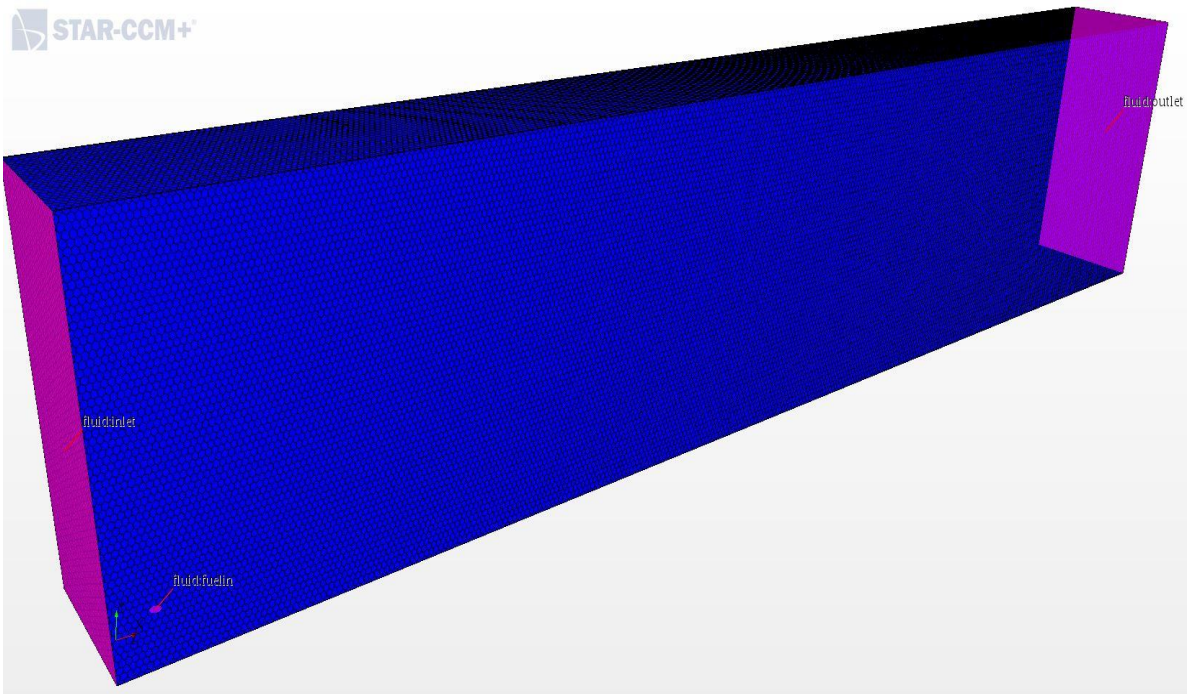Figure 9: Meshing image for crossflow CAD model with target base size of 4.7 mm and

Coflow CAD detailed mesh of the fuel inlet with target base size of 0.47 mm.

TURBULENCE, SOOT AND RADIATION MODELS USED.

- The RANS simulation was the turbulence model used, which was the k-ϵ, k-w and the SST turbulence model.

- Soot model used was one-step, two-step, and the Moss & Brookes model.

- Radiation model was the P1 model, Rosseland model, and no radiation.

- With gravity and no gravity model (gravity in negative Y-direction).

RANS TURBULENCE MODEL

Since balance equations for mean quantities in RANS are obtained by average instantaneous balance equations. The beginning point for instantaneous balance equations for mass, species, momentum, and enthalpy as shown in equation 1 to 4, the average balance equation become;

- Mass; $\dfrac{\partial \bar{\rho}}{\partial t} + \dfrac{\partial}{\partial x_i}(\bar{\rho}\tilde{u}_i) = 0$ (27)

- Momentum; $\dfrac{\partial \bar{\rho}\tilde{u}_i}{\partial t} + \dfrac{\partial}{\partial x_i}\left(\bar{\rho}\tilde{u}_i\tilde{u}_j\right) + \dfrac{\partial \bar{\rho}}{\partial x_j} = \dfrac{\partial}{\partial x_i}\left(\overline{\tau_{\iota J}} - \bar{\rho}\widetilde{u_\iota''}\widetilde{u_j''}\right)$ (28)

- Chemical species;

$$\frac{\partial(\bar{\rho}\tilde{Y}_k)}{\partial t} + \frac{\partial}{\partial x_i}\left(\bar{\rho}\tilde{u}_i\tilde{Y}_k\right) = -\frac{\partial}{\partial x_i}\left(\overline{V_{k,\iota}Y_k} + \bar{\rho}\widetilde{u_\iota''}\widetilde{Y_k''}\right) + \overline{\dot{\omega}_k} \text{ for k} = 1,\text{N}$$ (29)

- Enthalpy;

$$\frac{\partial \bar{\rho}\tilde{h}_s}{\partial t} + \frac{\partial}{\partial x_i}\left(\bar{\rho}\tilde{u}_i\tilde{h}_s\right) = \overline{\dot{\omega}_T} + \frac{\overline{Dp}}{Dt} + \frac{\partial}{\partial x_i}\left(\lambda\frac{\partial T}{\partial x_\iota} - \overline{\rho u_\iota'' h_s''}\right) + \overline{\tau_{\iota J}\frac{\partial u_\iota}{\partial x_J}} -$$

$$\frac{\partial}{\partial x_i}\left(\rho \sum_{k=1}^{N} V_{k,\iota}Y_k h_{s,k}\right)$$ (30)

Where;

$$\frac{\overline{Dp}}{Dt} = \frac{\partial \bar{p}}{\partial t} + \overline{u_\iota \frac{\partial p}{\partial x_\iota}} = \frac{\partial \bar{p}}{\partial t} + \tilde{u}_i \frac{\partial \bar{p}}{\partial x_i} + \overline{u_\iota'' \frac{\partial p}{\partial x_\iota}} \qquad (31)$$

These equations are similar to the original reynolds averaged equations for constant density flows. There are various turbulence model in RANS, but only these few will be discussed because of its use for the research, and they are two equation models;

- K-epsilon (k-ϵ)

- K-omega (k-ω)

- Shear stress transport (SST) model

K-epsilon (k-ϵ) turbulent model

The K-epsilon model us the most common turbulence model, but it doesn't perform well in cases of large adverse pressure gradient [10]. The two equation model accounts for mechanisms that affect the convection and diffusion of turbulent energy. The first variable is turbulent kinetic energy,k, predicts the energy of the turbulence while the second variable is turbulent dissipation, ϵ, predicts the scale of turbulence. The turbulence model developed by Launder and Sharma is called the standard k-epsilon model and the two equations are partial differential equations. [11].

The transport equation for standard k-epsilon model

For turbulent kinetic energy;

$$\frac{\partial}{\partial t}(\rho k) + \frac{\partial}{\partial x_i}(\rho k u_i) = \frac{\partial}{\partial x_j}\left[\left(\mu + \frac{\mu_t}{\sigma_k}\right)\frac{\partial k}{\partial x_j}\right] + P_k + P_b - \rho \epsilon - Y_M + S_k \qquad (32)$$

For dissipation ϵ;

$$\frac{\partial}{\partial t}(\rho\epsilon) + \frac{\partial}{\partial x_i}(\rho\epsilon u_i) = \frac{\partial}{\partial x_j}\left[\left(\mu + \frac{\mu_t}{\sigma_\epsilon}\right)\frac{\partial\epsilon}{\partial x_j}\right] + C_{1\epsilon}\frac{\epsilon}{k}(P_k + C_{3\epsilon}P_b) - C_{2\epsilon}\rho\frac{\epsilon^2}{k} + S_\epsilon \quad (33)$$

Turbulent viscosity is modified as;

$$\mu_t = C_\mu\rho\frac{k^2}{\epsilon} \qquad (34)$$

Production of k;

$$P_k = -\rho\overline{u_i'u_j'}\frac{\partial u_j}{\partial x_i} \qquad (35)$$

$$P_k = \mu_t S^2 \qquad (36)$$

Where S is the modulus of the mean rate of strain tensor, defined as;

$$S \equiv \sqrt{2S_{ij}S_{ij}} \qquad (37)$$

Effect of buoyancy;

$$P_b = \beta g_i\frac{\mu_t}{Pr_t}\frac{\partial T}{\partial x_i} \qquad (38)$$

$$\beta = -\frac{1}{\rho}\left(\frac{\partial\rho}{\partial T}\right)_P \qquad (39)$$

Where Pr_t is the turbulent Prandtl number for energy, g_i is the gravitiational vector in the ith direction, and β is the coefficient of thermal expansion. For standard and realizable models, the default Pr_t is 0.85.

Model constants [12]

$$C_{1\epsilon} = 1.44; \ C_{2\epsilon} = 1.92; \ C_{\mu} = 0.09; \sigma_k = 1.0; \ \sigma_{\epsilon} = 1.3$$

<u>K-Omega (K-**ω**) Model</u>

This is also a two-equation turbulence model for RANS equations. the k-ω model just like

the k-ϵ model has two variables represented in two partial differential equations. The first

variable is the turbulent kinetic energy, k, which predicts energy in turbulence. The second

variable is the specific rate of dissipation, ω, which determines the scale of the turbulence.

There are various commonly used k-ω model which are;

- Standard Wilox's k-omega model

- Wilox's modified k-omega model

- SST k-omega model.

Standard Wilox's k –omega turbulence model, the k and ω are modeled as [13,14];

Kinematic eddy viscosity, $v_T = \dfrac{k}{\omega}$ (40)

Turbulent kinetic energy;

$$\frac{\partial k}{\partial t} + U_j \frac{\partial k}{\partial x_j} = \tau_{ij} \frac{\partial U_i}{\partial x_j} - \beta^* k\omega + \frac{\partial}{\partial x_j}\left[(v + \sigma^* v_T)\frac{\partial k}{\partial x_j}\right] \quad (41)$$

Specific rate of dissipation;

$$\frac{\partial \omega}{\partial t} + U_j \frac{\partial \omega}{\partial x_j} = \alpha \frac{\omega}{k} \tau_{ij} \frac{\partial U_i}{\partial x_j} - \beta\omega^2 + \frac{\partial}{\partial x_j}\left[(v + \sigma v_T)\frac{\partial \omega}{\partial x_j}\right] \quad (42)$$

Closure coefficients and other relations

$$\alpha = \frac{5}{9}; \ \beta = \frac{3}{40}; \ \beta^* = \frac{9}{100}; \ \sigma = \frac{1}{2}; \ \sigma^* = \frac{1}{2}; \ \varepsilon = \beta^*\omega k$$

SST (Menter's shear stress transport) turbulence model

This two equation eddy-viscosity model combines the k-ω and k-ϵ model. The k-omega model is used in the inner boundary layer, all the way down to the wall through the viscous sub-layer, hence can be used as a low Reynold turbulence model. While the k-epsilon model is used to predict the behavior of the free stream, and therefore avoids the k-omega problem. Menter (1993) [15] and Menter (1994) [16] explained the equations and closure coefficients and auxiliary equations for the SST model.

SOOT MODELLING

Three soot model in FLUENT (ANSYS software), used for this research study are the one-step method, the two-step method, and Moss&Brookes soot formation model.

One-step soot formation model

ANSYS Fluent uses the one-step Khan and Greeves model [26] to solve a single transport equation for the soot mass fraction.

$$\frac{\partial}{\partial t}[\rho Y_{soot}] + \nabla.[\rho \vec{v} Y_{soot}] = \nabla.\left[\frac{\mu_t}{\sigma_{soot}} \nabla Y_{soot}\right] + \mathcal{R}_{soot} \qquad (43)$$

Y_{soot} is soot mass fraction, σ_{soot} is turbulent Prandtl number for soot transport and $\mathcal{R}_{soot}$ is net rate of soot generation (kg/m^{3}s).

The two-step soot formation model

This model predicts the generation of radical nuclei and also computes the formation of soot on these nuclei. The two-step model developed my Tenser et al [27], is used in ANSYS Fluent to solve transport equations for two scalar quantities, which are the soot mass fraction, and the normalized radical nuclei concentration.

$$\frac{\partial}{\partial t}[\rho b_{nuc}^*] + \nabla.[\rho \vec{v}\, b_{nuc}^*] = \nabla.\left[\frac{\mu_t}{\sigma_{nuc}}\nabla b_{nuc}^*\right] + \mathcal{R}_{nuc}^* \qquad (44)$$

b_{nuc}^* is normalized radical nuclei concentration (particles $\times 10^{-15}$/kg), σ_{nuc} is turbulent Prandtl number for nuclei transport, and $\mathcal{R}_{nuc}^*$ is normalized net rate of nuclei generation (particles $\times 10^{-15}$/m^3 -s).

Moss and Brookes Model

The Moss-Brookes model solves transport equations for soot mass fraction, Y_{soot} and the normalized radical nuclei concentration, b_{nuc}^* [21].

$$\frac{\partial}{\partial t}[\rho Y_{soot}] + \nabla.[\rho \vec{v} Y_{soot}] = \nabla.\left[\frac{\mu_t}{\sigma_{soot}}\nabla Y_{soot}\right] + \frac{dM}{dt} \qquad (45)$$

$$\frac{\partial}{\partial t}[\rho b_{nuc}^*] + \nabla.[\rho \vec{v}\, b_{nuc}^*] = \nabla.\left[\frac{\mu_t}{\sigma_{nuc}}\nabla b_{nuc}^*\right] + \frac{1}{N_{norm}}\frac{dN}{dt} \qquad (46)$$

Where M is soot mass concentration (kg/m^3), $N_{norm} = 10^{15}$ particles.

Moss-Brookes model was mainly developed and validated for methane flames, and Fenimore and Jones [61] proposed its oxidation model. An extension for higher hydrocarbon fuels called the Moss-Brookes-Hall model. The extended version is a model reported by Wen et al. [62], based on model extensions proposed by Hall et al. [63] and an oxidation model proposed by Lee et al. [64]. Moss-Brookes assumption of a soot inception due to acetylene or benzene (for higher hydrocarbons), while Hall [63] is based on a soot inception rate due to two-ringed and three-ringed aromatics. The Fenimore-Jones model assumes that the hydroxyl radical (OH) is the dominant oxidizing agent or the soot oxidation term, while Lee model assumes oxygen, O_2 , also as an oxidation term.

RADIATION MODELLING

The P₁ Model Equations

The P$_1$ model reduces the integral terms of RTE to differential terms via a finite set of moment equations [28]. To develop the general PN method, the radiation intensity at each position is expressed as an expansion in a series of orthogonal harmonics, and the series is truncated after a finite number of N terms. [29,30].

The P$_1$ model is the simplest case of P$_N$ model if only four terms are retained. The P1 model should typically be used for spectral optical thickness $\kappa_\lambda > 1$ [31]. the following equation is obtained for radiation flux, q$_r$ [32]:

$$q_r = -\frac{1}{3(a + \sigma_s) - C\sigma_s} \nabla G \qquad (47)$$

Here a is absorption coefficient, σ_s is the scattering coefficient, G is the incident radiation, and C is the linear-anisotropic phase function coefficient. Introducing the parameter, Γ,

$$\Gamma = \frac{1}{3(a + \sigma_s) - C\sigma_s}, \qquad then \quad q_r = -\Gamma \nabla G \;..... \qquad (48)$$

The transport equation for G is

$$\nabla.(\Gamma \nabla G) - aG + 4a\sigma T^4 = S_G \;.....(49)$$

Where σ is the Stefan-Bolzmann constant, and S_G is a local radiation source term. Combining equations (48&49) gives expression $-\nabla.q_r$, which can be substituted into the energy equation to account for heat sources (sinks) due to radiation.

$$-\nabla.q_r = a(G - 4\sigma T^4) = (G - 4\pi I_b) \qquad (50)$$

Where I_b is black body isotropic intensity.

Rosseland radiation model

Rosseland model is also known as the diffusion approximation model. we consider an absorbing and emitting medium with isotropic scattering ($\phi_\lambda = 1$). In an optically thick medium ($(a + \sigma_s)L \gg 1$), radiation travels in a short distance before being absorbed or scattered. The Rosseland approximation shows that the local spectral intensity, I_λ depends on the magnitude and the gradient of the local blackbody spectral intensity, $I_{\lambda b}$(T), at that position [28]. The radiative flux vector for the grey medium is approximated as;

$$q_r = -4\pi\Gamma\frac{\partial I_b(T)}{\partial x_i} = -16\sigma\Gamma n^2 T^3 \frac{\partial T}{\partial x_i} = -16\sigma\Gamma n^2 T^3 \nabla T = -\Gamma.\nabla G \qquad (51)$$

Where n is the refractive index.

CHAPTER FOUR: RESULTS AND DISCUSSION.

COFLOW RESULTS

In this chapter, the results were obtained from numerical simulations. The data line used along the xy plane, for generating the results were located at the center of the axis. Note we did not tune any coefficients in the models used (turbulent, soot and radiation) in both coflow and crossflow simulations.

The results obtained were compared to the Coppalle and Joyeux [50] experiment and Santu simulation. From Santu [51] work, he concluded that the best model suitable for his work and closer to the experimental results was one-step soot model, SST turbulence model and Rosseland radiation model with gravity.
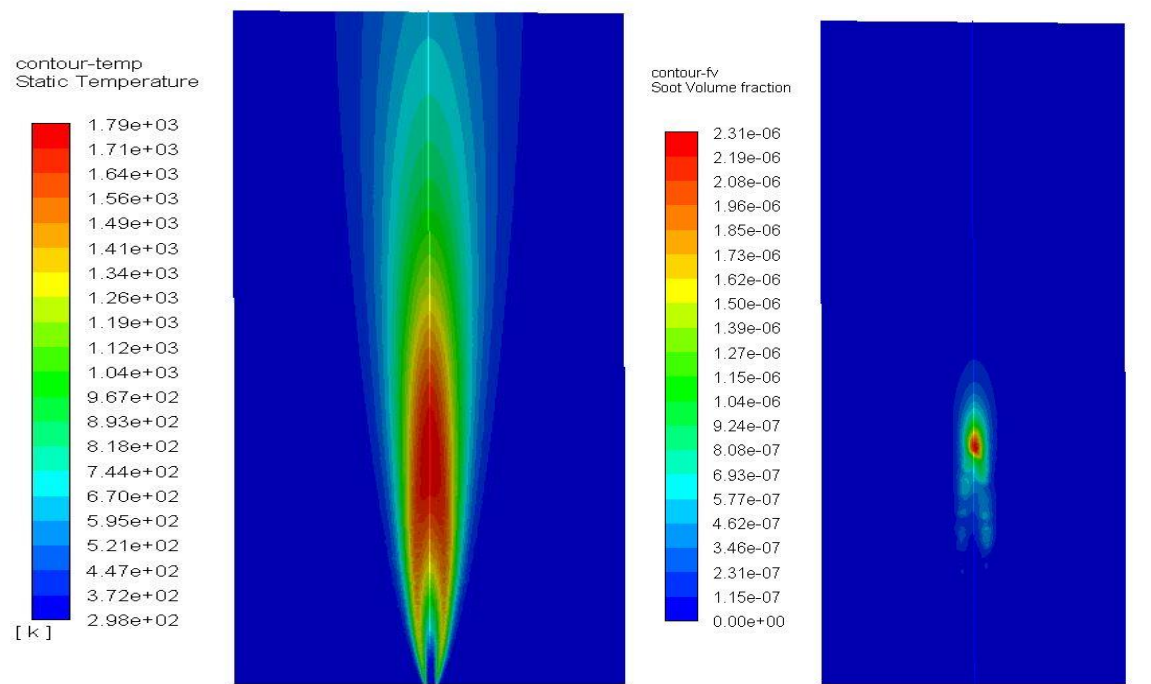
Figure 10: Temperature and soot volume fraction for one step-SST-Rosseland model with Gravity.

Comparing the turbulence model, at the recommended soot and radiation model which is one-step soot model and Rosseland radiation model with gravity, we have;
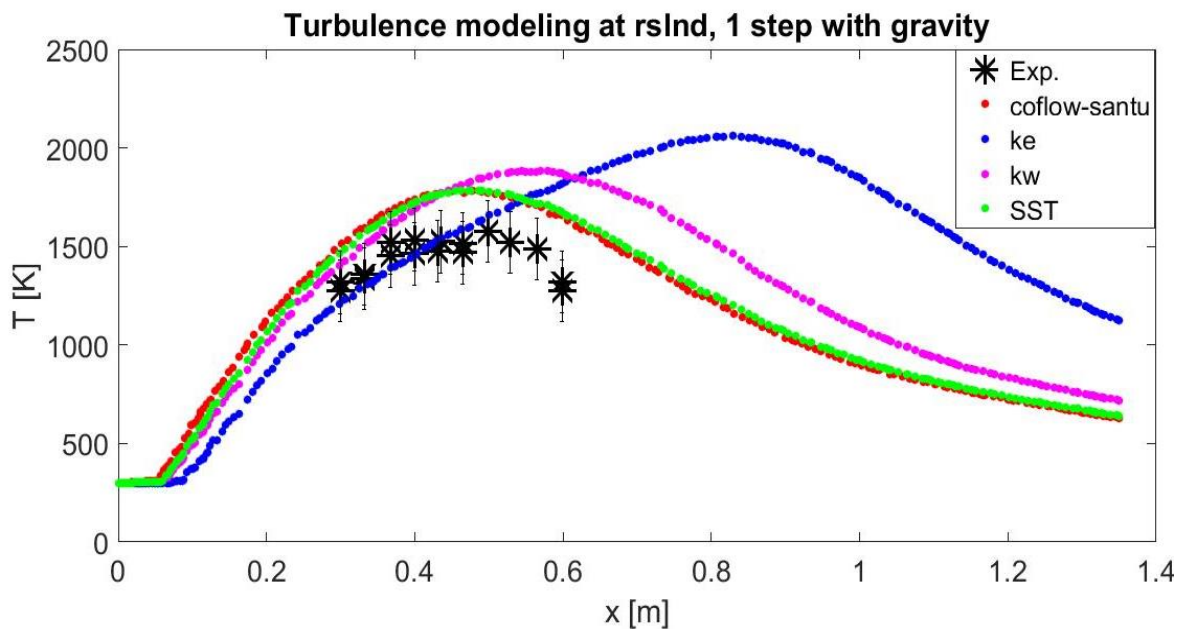

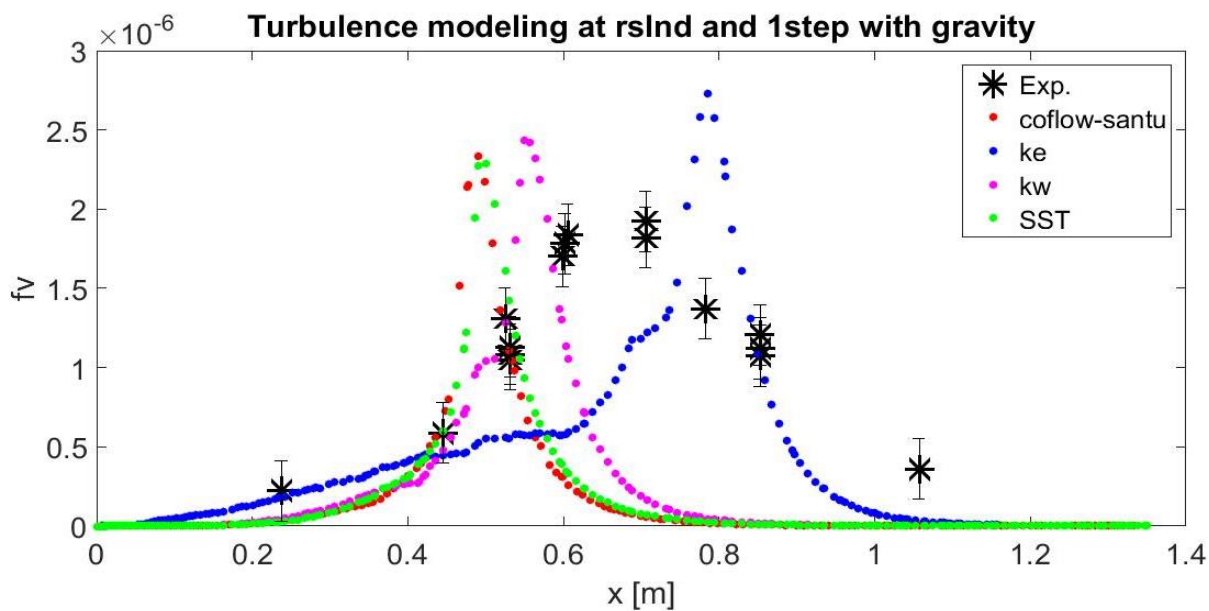Figure 11: A plot of temperature showing different turbulent models.

Figure 12: A plot of soot volume fraction showing different turbulent models.

The error bar at the experiment data is about 10% error of the maximum temperature and soot volume fraction of the experimental result, which is 157K and 0.192 e^{-6} respectively.

From figure 11, the SST model shows the temperature is in a reasonable agreement to the experimental result and was coincides with the Santu model. The experiment and simulated results maximum temperatures are almost at similar location along the axis. The k-ϵ model gave very high temperature and its maximum temperature location on the axis is furthest away as compared to the other models. From figure 12, soot production closest to the experimental data was the SST model, which also coincides with santu model, although experimental and simulated results maximum soot production are almost at a different location along the axis. Overprediction of soot production by k-ϵ model was also observed.

Also comparing the soot model, at Rosseland radiation model, SST turbulent model and with gravity we have;
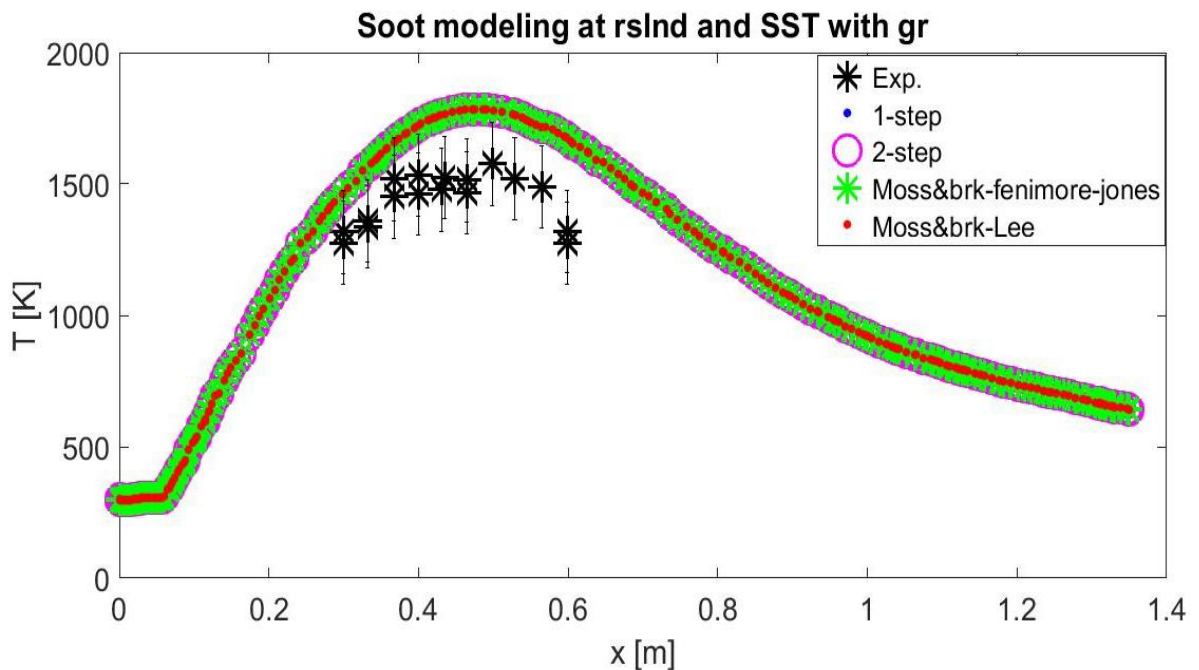

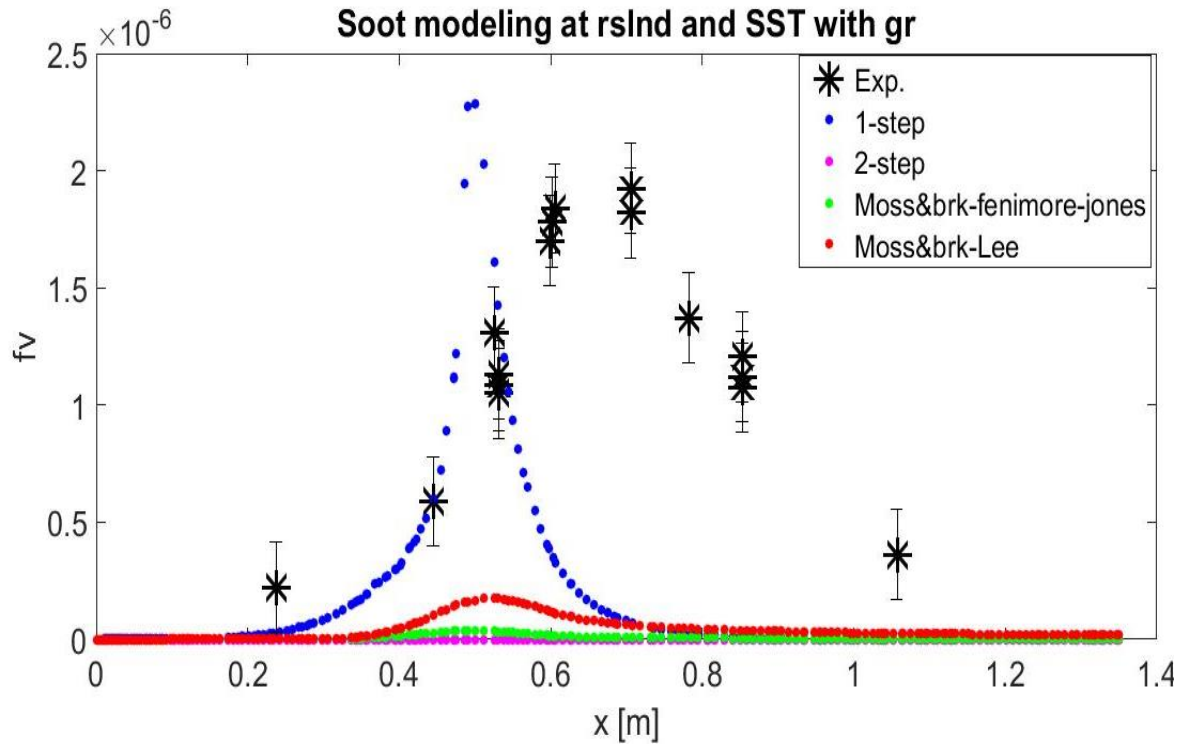Figure 13: A plot of temperature showing different soot models.

Figure 14: A plot of soot volume fraction showing various soot models.

Figure 13 shows that at various soot model, the temperature is the same along the axis location., as they coincide. The various soot model did not affect temperature but just the soot production as indicated in figure 14. The one-step model gave the best prediction, although the location of soot production varies along the axis. The Moss&Brookes model with Lee oxidation gave a better prediction compared to the Fenimore-Jones oxidation model.

Comparing the radiation model at one-step soot model, and SST turbulent model with gravity. The model with no radiative heat transfer also has no gravity model.
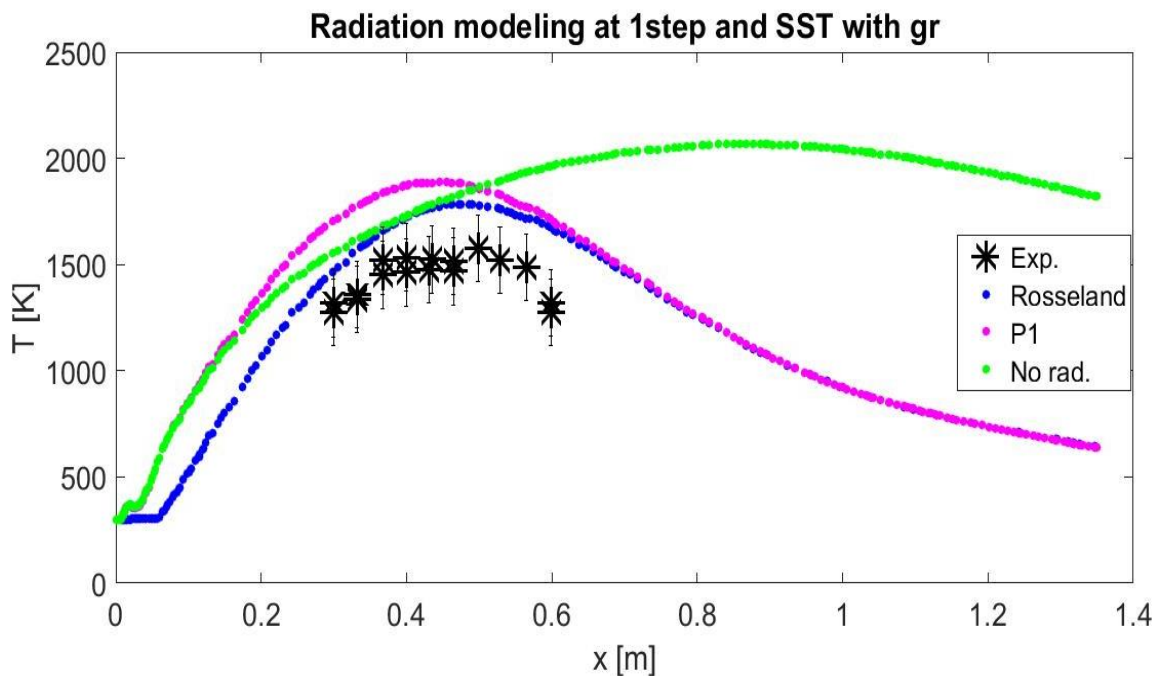
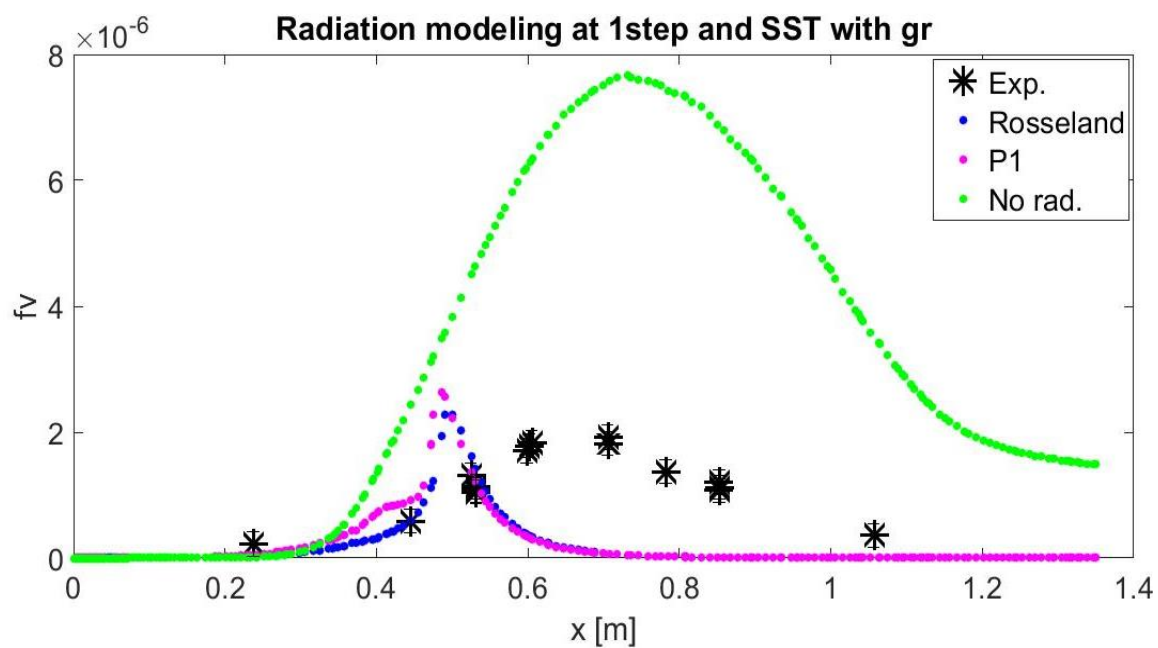Figure 15: A plot of temperature showing effect of various radiation models.

Figure 16: A plot of soot volume fraction showing effect of various radiation models.

Figure 15&16 shows Rosseland radiation model gave the best prediction, as compared to P_1 model. It is observed the overprediction in temperature with model with no radiative heat transfer and no gravity, which leads to significant increase in soot producution (roughly a 4× factor). While figure 16, also shows Rosseland gave best prediction for soot production.

Comparing gravity and no gravity, using SST, one step and Rosseland model, also compared to Santu [51] model with gravity we have;
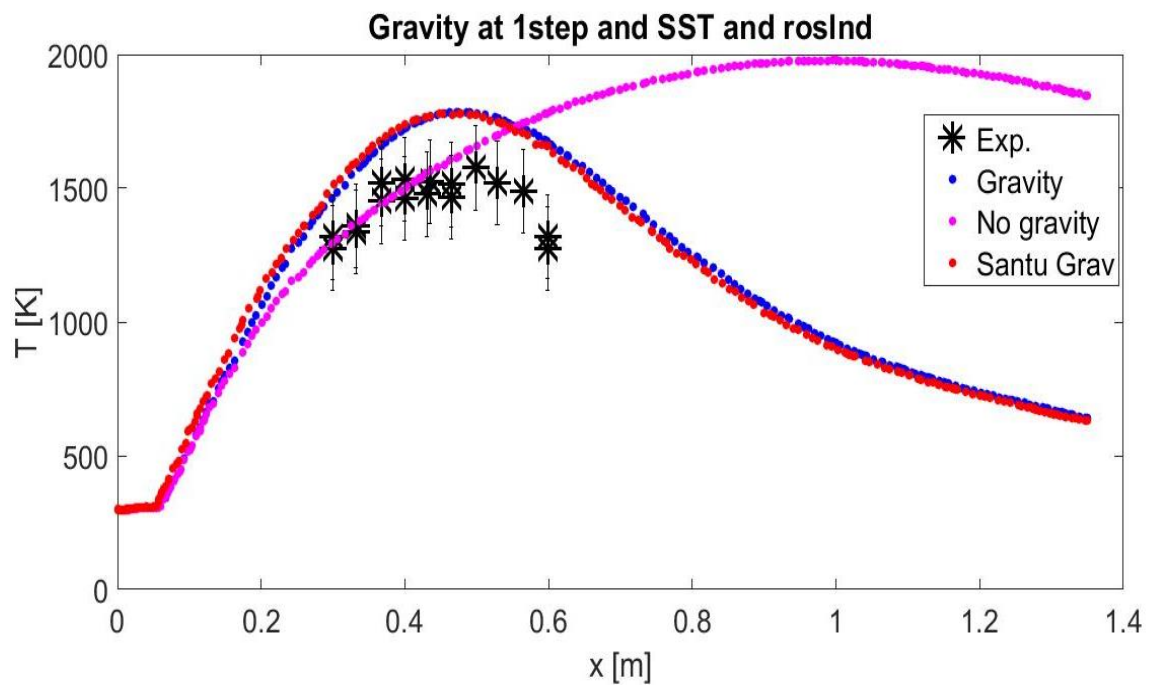

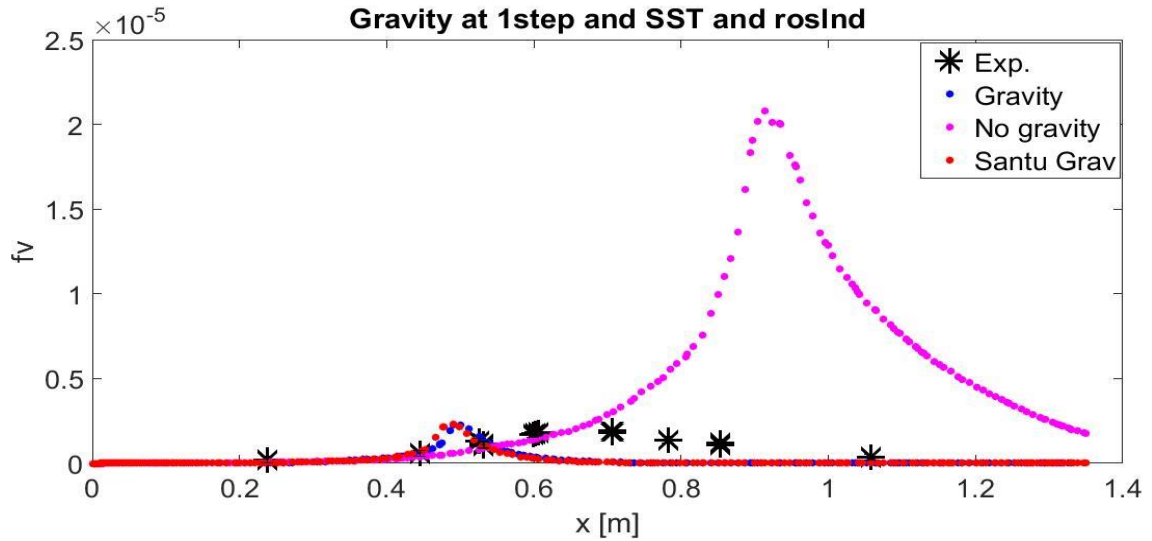Figure 17: A plot of temperature showing with and without gravity effect.

Figure 18: A plot of soot volume fraction showing with and without gravity effect.

It is observed fom figure 17&18 that the model with absence of gravity lead to significant increase in temperature, which lead to significant increase in soot production (roughly a 10× factor).

Comparing Moss&Brookes using Lee oxidation soot model, at various turbulent and radiation model, with gravity;
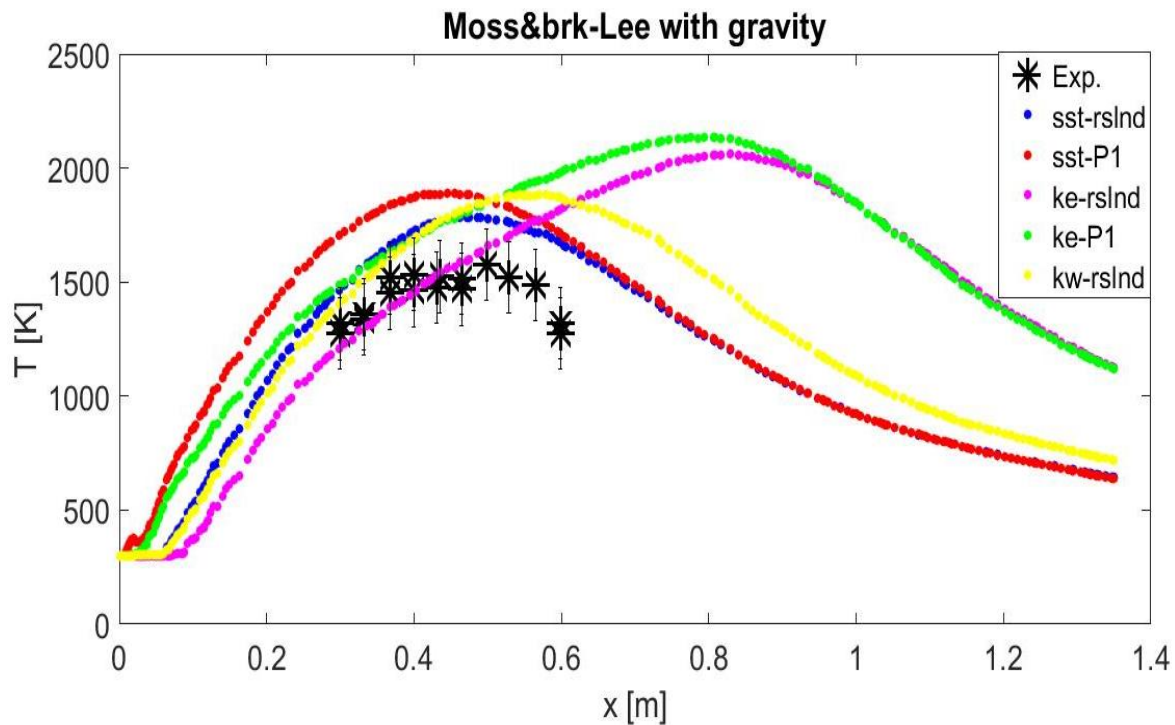
Figure 19: A plot of temperature with Moss&Brookes with Lee oxidation model using various turbulent and radiation model, with gravity.
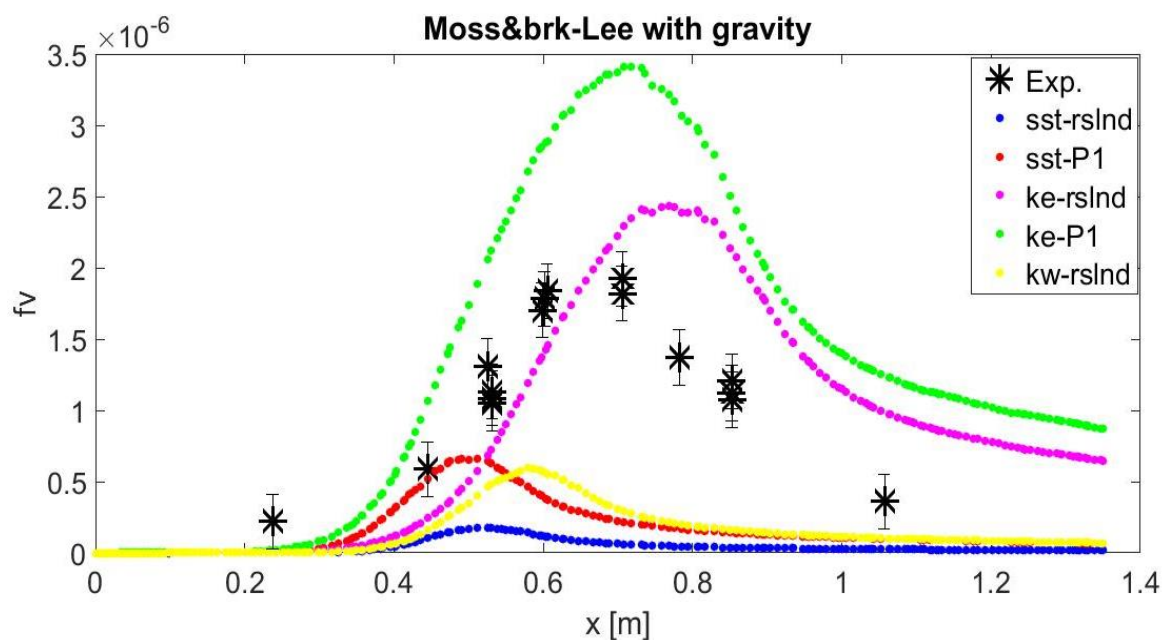

Figure 20: A plot of soot volume fraction with Moss&Brookes with Lee oxidation model using various turbulent and radiation model, with gravity.

The model that gave the best temperature prediction was SST-Rosseland model, which was first observed in figure 13. That irrespective of soot model SST- Rosseland model gave the most reasonable prediction. For the soot production, k-epsilion model with Rosseland radiation model at Moss&brook with Lee oxidation gave the best prediction. Lorenzo et al [38] found out Moss-Brookes method with k-ϵ turbulent model and his radiation model was discrete ordinate method was a better model to predict soot formation for turbulent diffusion flame using n-Decane (in stoichiometric ratio with toluene) as fuel and air as the oxidizer. Further work could be done here using other radiation models to know if better results could be generated.

Table 1 is generated to compare the differences in maximum values of the various models with the maximum temperature of the experimental result, 1576K, and maximum soot volume fraction obtained $1.923e^{-6}$.

Table 1: Comparing differences in maximum values from the experimental maximum values.

Model	Maximum temperature [K]	% error from experiment	Maximum soot volume fraction	% error from experiment
Santu-one-step SST-Rosseland-gravity	1781	13%	2.335 e^{-6}	21.4 %
One-step-SST-Rosseland-gravity	1785	13.3%	2.285 e^{-6}	18.8 %
M&Brk-Lee-k-eps & Rosseland-gravity	2063	30.9 %	2.432 e^{-6}	26.5 %

From the results generated the one-step soot model with SST turbulent model and Rosseland radiation with gravity gave the best prediction and in reasonable agreement with the experimental results, just as Santu predicted. From Table 1 indicates the soot production from the study is slightly lower than that from Santu simulation

CROSSFLOW RESULTS

Applying the one-step-SST-Rosseland model with radiation to crossflow jet flame, at various velocity ratios.

$$Velocity\ ratio = \frac{velocity\ of\ jet\ (fuel\ inlet)\ [m/s]}{velocity\ of\ the\ crossflow\ (air\ inlet)\ [m/s]}$$

The data values for the crossflow were collected, where the maximum values existed across the axis and varies for different velocity ratios due to differences in the flame front. Illustrations are shown the images below;
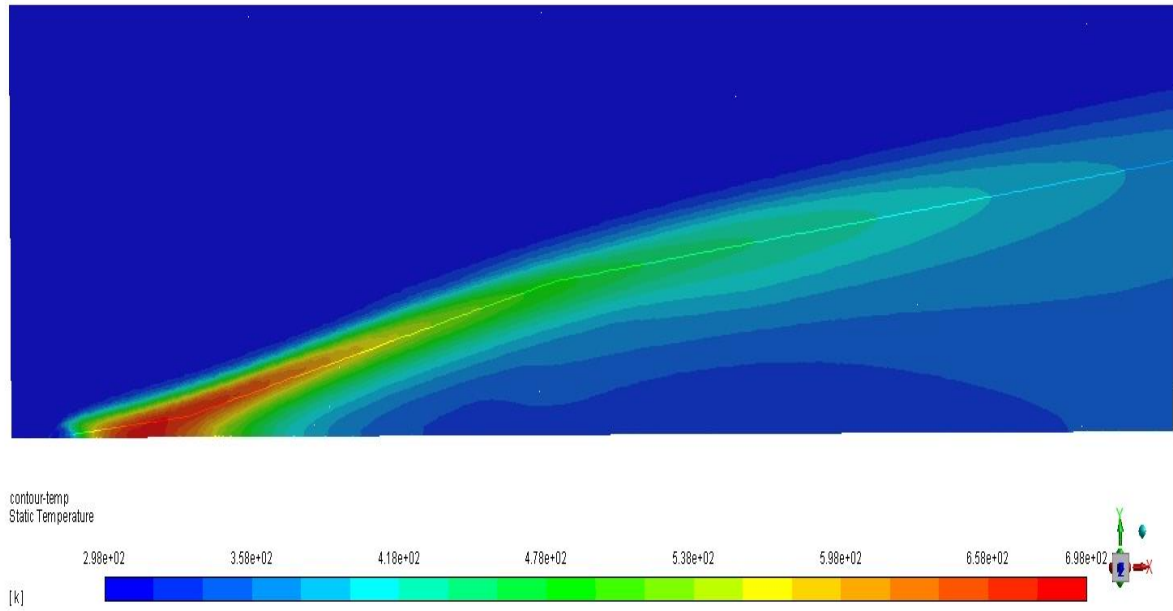
For velocity ratio of 0.5

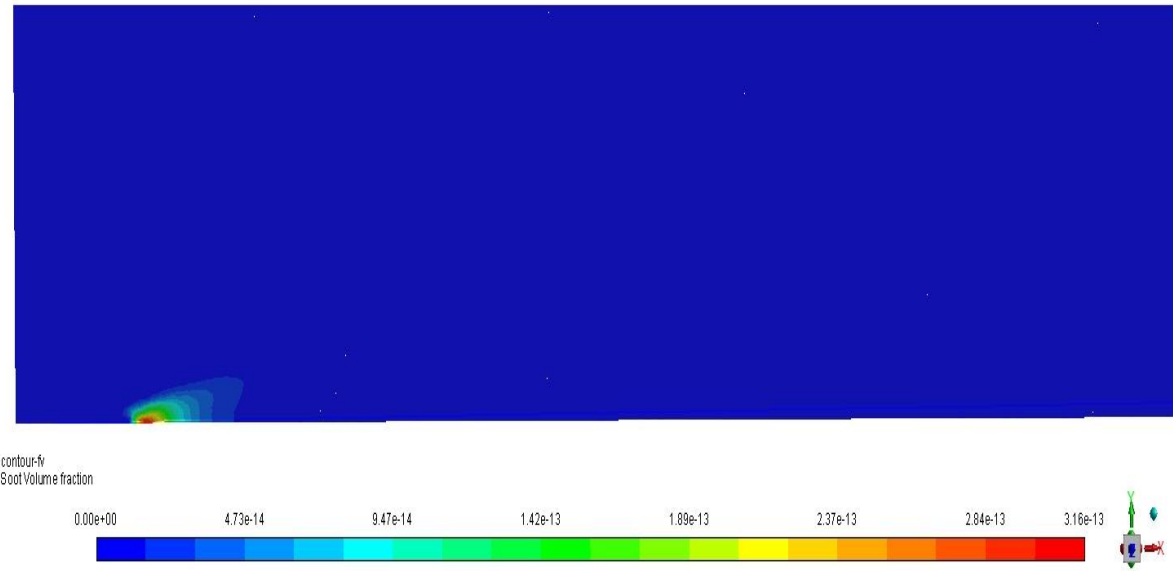Figure 21: Contour plot of temperature at velocity ratio of 0.5.

Figure 22: Contour plot of soot volume fraction at velocity ratio of 0.5.
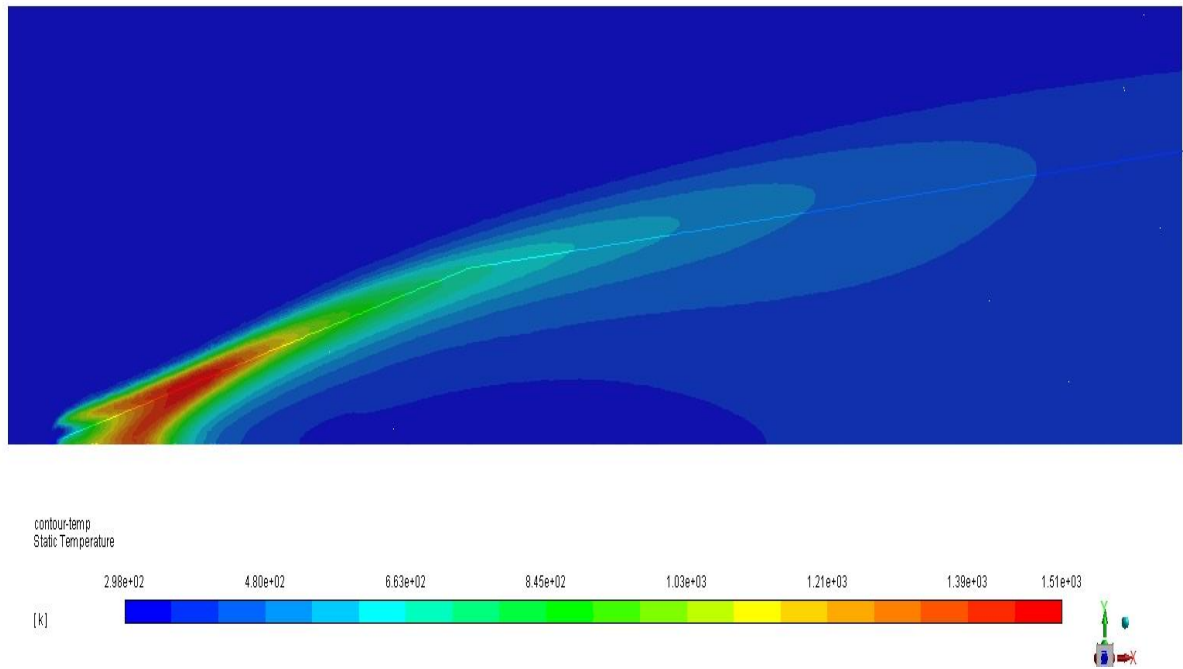
For velocity ration of 1

Figure 23: Contour plot of temperature at velocity ratio of 1.
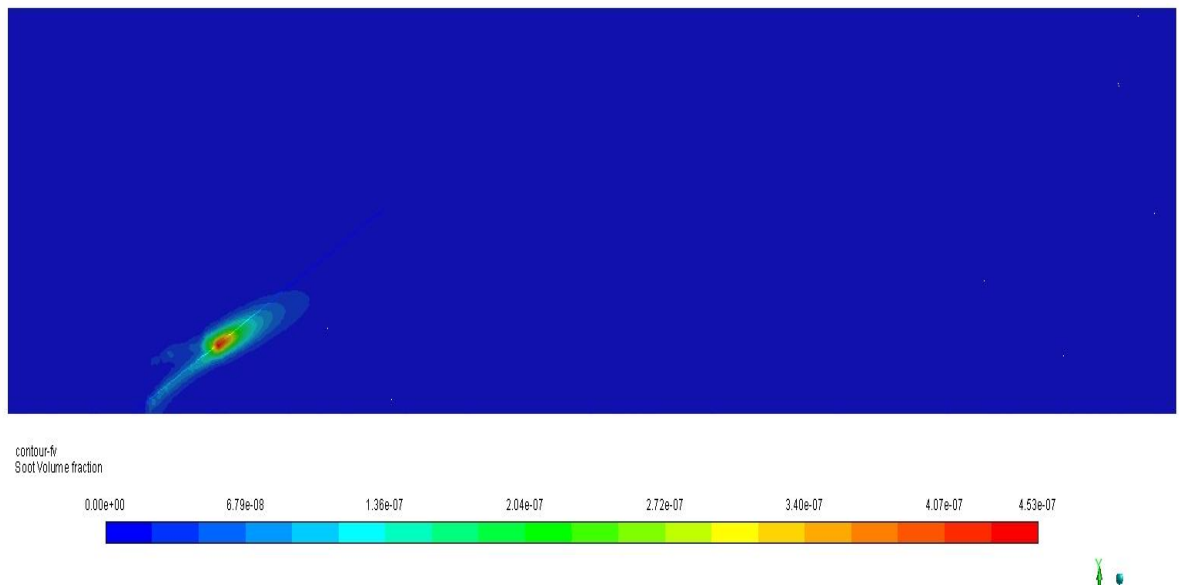

Figure 24: Contour plot of soot volume fraction at velocity ratio of 1.
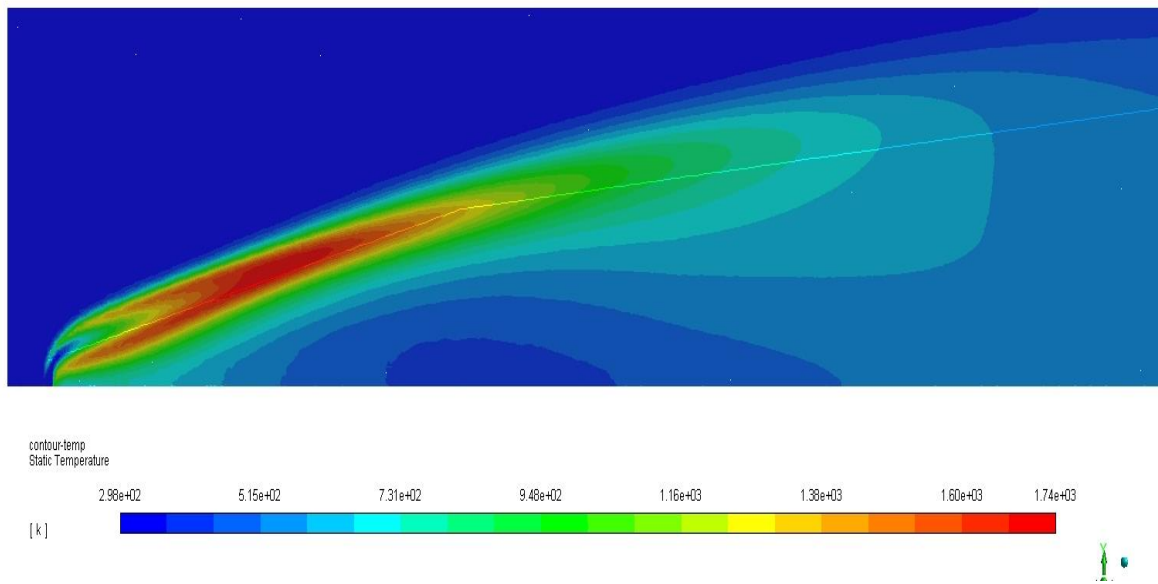
For velocity ration of 3

Figure 25: Contour plot of temperature at velocity ratio of 3.

Figure 26: Contour plot of soot volume fraction at velocity ratio of 3.

For velocity ration of 6.3

contour-temp
Static Temperature

2.98e+02   5.34e+02   7.71e+02   1.01e+03   1.24e+03   1.48e+03   1.72e+03   1.87e+03

[k]

Figure 27: Contour plot of temperature at velocity ratio of 6.3.

contour-fv
Soot Volume fraction

0.00e+00   7.16e-07   1.43e-06   2.15e-06   2.87e-06   3.58e-06   4.30e-06   4.78e-06

Figure 28: Contour plot of soot volume fraction at velocity ratio of 6.3.

For velocity ration of 10

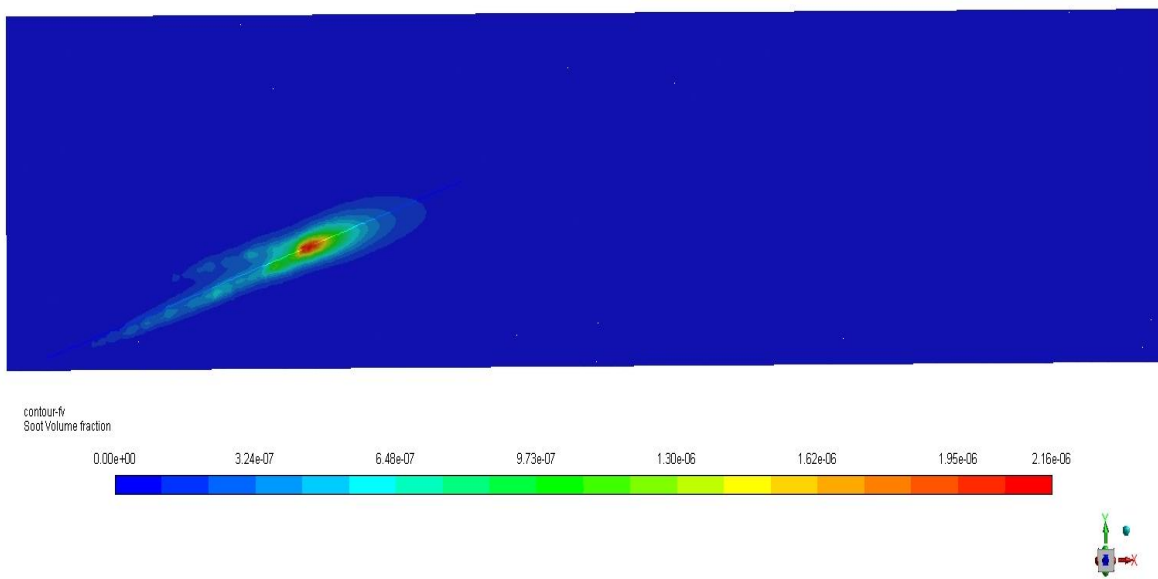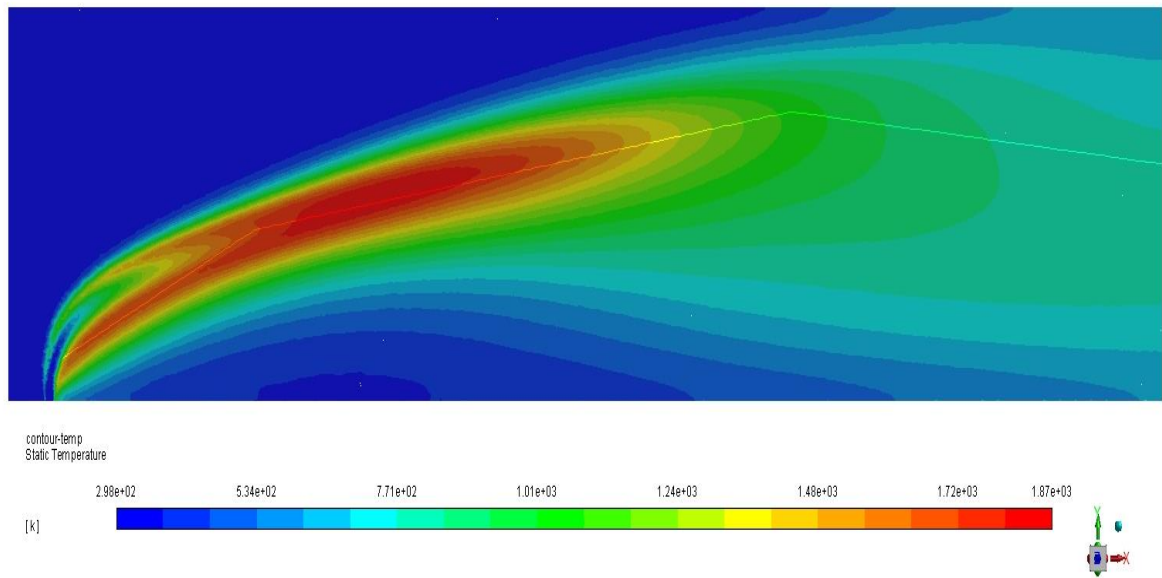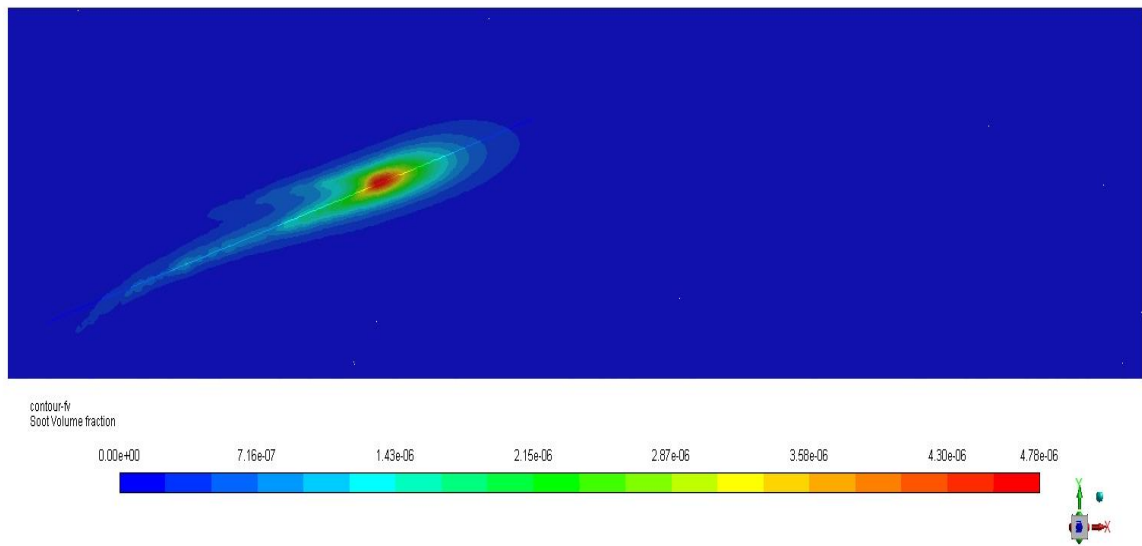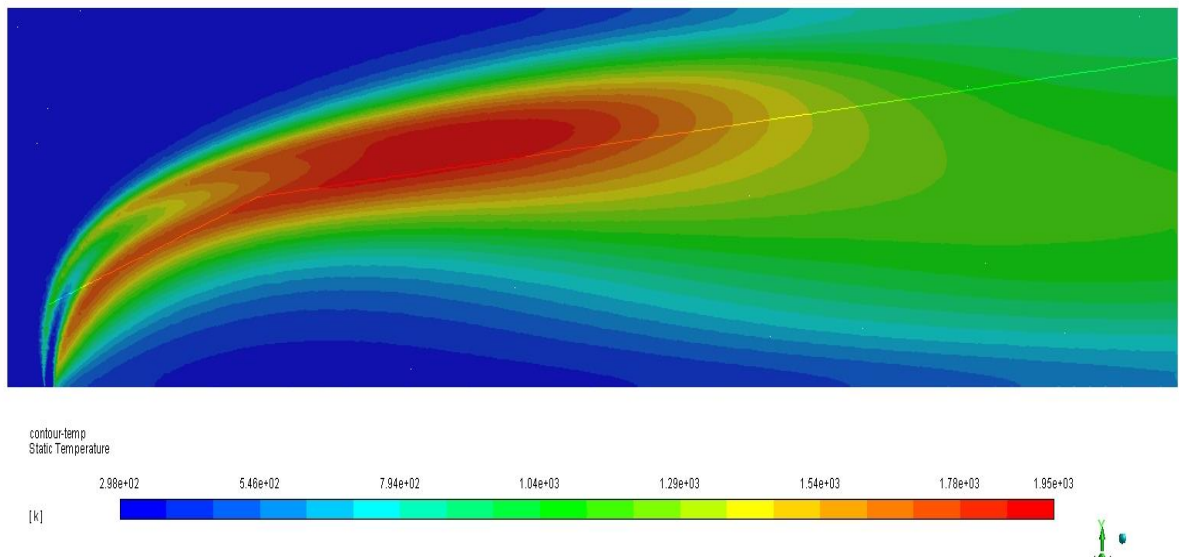Figure 29: Contour plot of temperature at velocity ratio of 10.
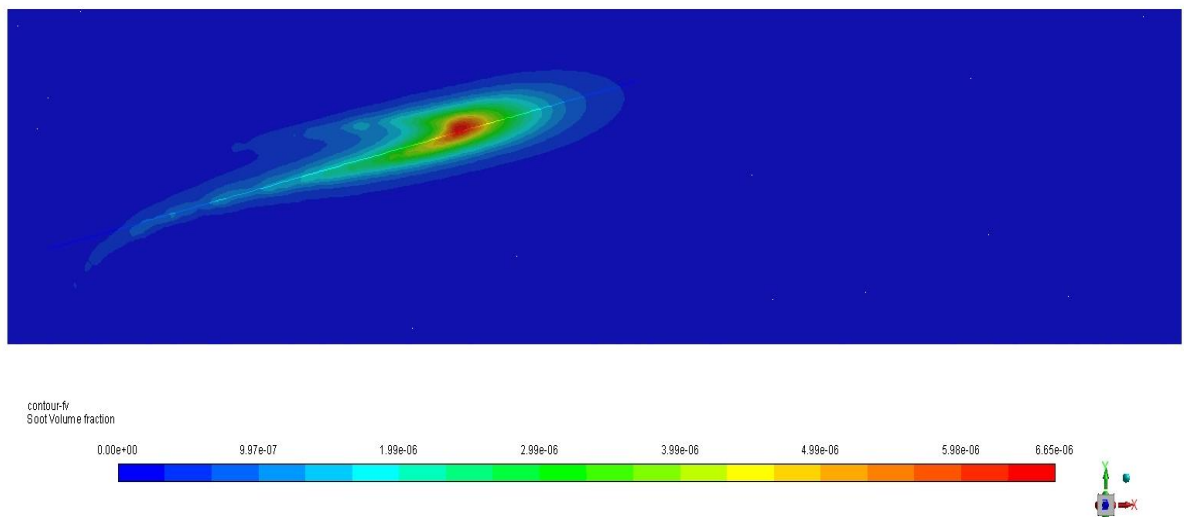
Figure 30: Contour plot of soot volume fraction at velocity ratio of 10.

The temperature and soot volume fraction data was collected with the data line indicated

in the images and plotted as shown in figure 29&30.

one step, SST, Roseland model with gravity in crossflow
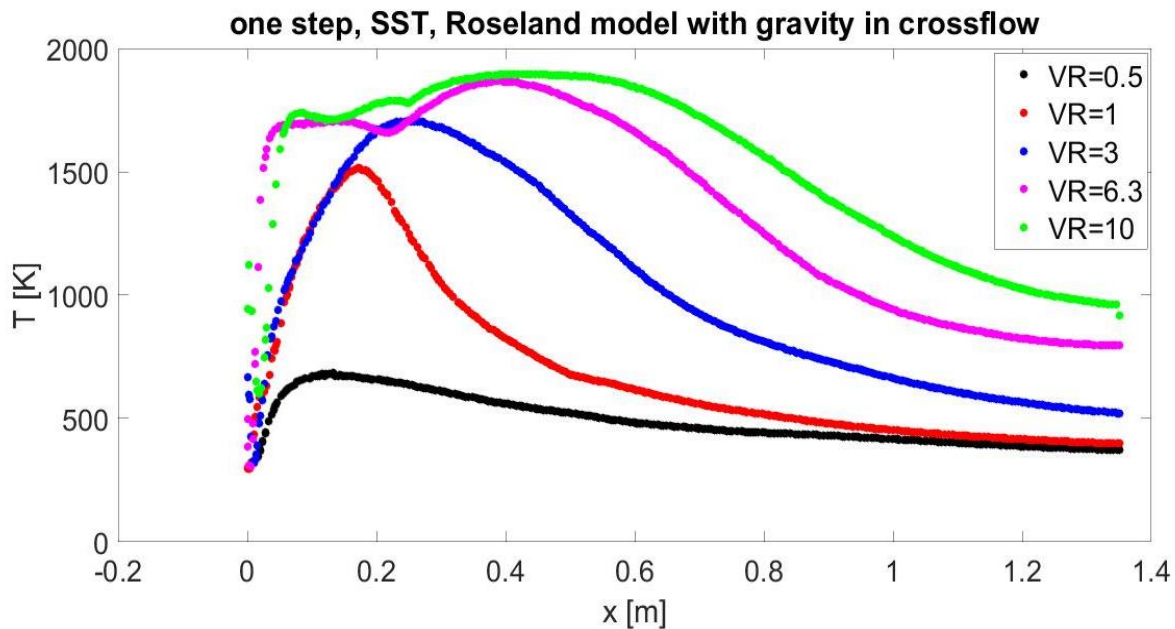
Figure 31: Plot of temperatures at various velocity ratios.

one step, SST, Roseland model with gravity in crossflow

Figure 32: Plot of soot volume fraction at various velocity ratios.

It is interesting to observe that as velocity ratio increases the temperature and soot production increases also. This is due to significant increase in fuel concentration. The

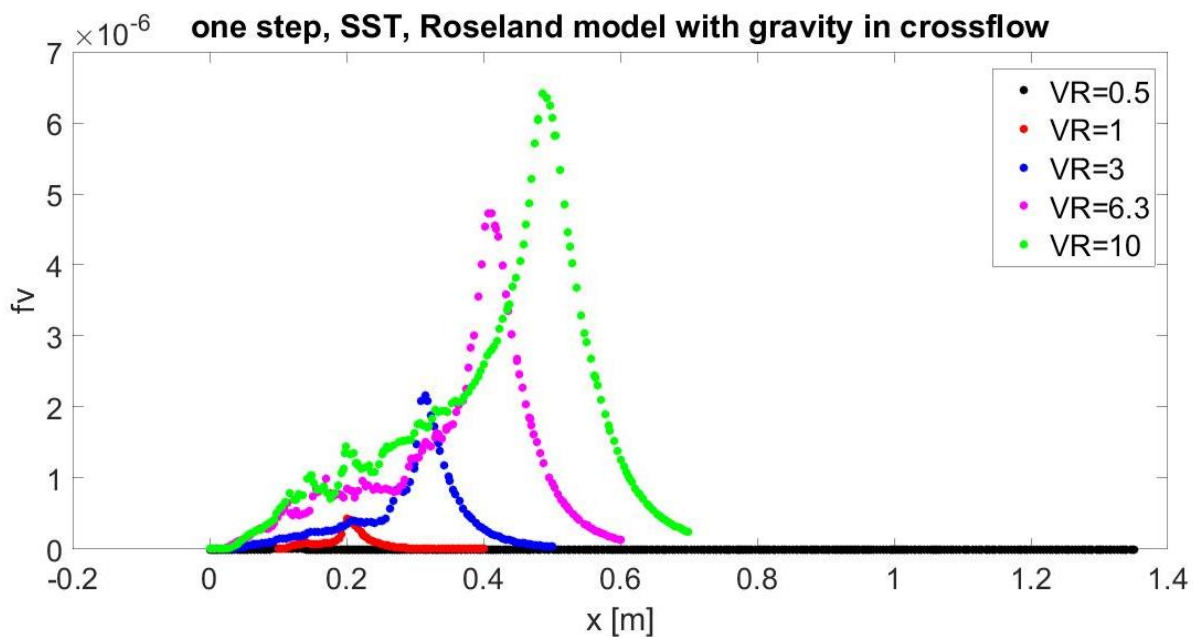temperature for VR=0.5 is too low, and possible complete combustion did not occur, as the soot volume fraction is also very low with the value of $3.118\ e^{-13}$. For VR = 1, the concentration of oxidizer (air), will be very high. When combustion occurs, most of the soot is easily oxidized and soot production is minimized.

Temperature is maximum at the reaction zone, and the reaction is dependent on the concentration of fuel and oxidizer. At lower fuel concentrations, heat released from reaction zone will be lower, therefore results in lower temperatures. Which explains the reason why temperature was increased as velocity ratio increases. Generally, an increase in temperature will lead to an increase in soot production.

Lignell et al summarized in his study that enhanced turbulent mixing of fuel and oxidizer stream had an effect on transport of soot particles towards the flame zone and location of soot directly impacts the temperature and gas composition that soot experiences, and therefore its radiative heat transfer and reaction rates [33,45].

It is also observed the location of maximum temperature and soot concentrations increases along the axis as velocity ratio increases. The maximum temperature is achieved in close proximity to fuel inlet at lower velocity ratios, where the reaction zone is located, and this is possible due to mixing between fuel and air streams. Therefore mixing of fuel and air is achieved in closer proximity to the inlet at lower velocity ratios. The location for maximum soot volume fraction is dependent on location of maximum temperature, hence its reaction rates.

Table 2: Comparing results obtained from various velocity ratios

Velocity ratio	Maximum temperature [K]	Location (m)	Maximum soot volume fraction	Location (m)
0.5	684	0.13	$3.118 \, e^{-13}$	0.10
1	1514	0.17	$4.354 \, e^{-7}$	0.20
3	1706	0.25	$2.161 \, e^{-6}$	0.31
6.3	1868	0.39	$4.734 \, e^{-6}$	0.41
10	1897	0.41	$6.413 \, e^{-6}$	0.49

It is interesting to observe that the coflow simulation which was at velocity ratio of 6.3, when compared to it crossflow at velocity ratio of 6.3, its temperature increased in crossflow, and the soot volume fraction also increased (roughly 2× factor).

Table 3: Results at velocity ratio of 6.3 for one-step-SST-Rosseland model with gravity

Type	Maximum temperature	Location from fuel inlet (m)	Maximum soot volume fraction	Location from fuel inlet (m)
coflow	1785	0.48	$2.285 \, e^{-6}$	0.5
crossflow	1868	0.39	$4.734 \, e^{-6}$	0.41

This may be as a result of mixing of fuel and air streams, which arises from different direction of air and fuel stream. The increase may be as a result of inadequate mixing in crossflow, as compared to coflow. The inadequate mixing of fuel and air stream can affect

reaction, and reduce oxidizer concentration, leading to increase in soot production and temperature increase.

VALIDATION

Validation is performed on the coflow simulation by comparing Coppalle and Joyeux experimental results and Santu simulation result to verify the best turbulent, soot and radiation model that best agrees with the experimental result.

Table 4: Summary of process variables and results in validation case and current case.

	Current study (coflow study)	Validation case (Coppalle & Joyeux experiment)
Velocity of fuel	6.3 m/s	6.3 m/s
Diameter of fuel inlet	9 mm	9 mm
Max. soot volume fraction	$2.29\ e^{-6}$	$1.92\ e^{-6}$
Max. Temperature	1785 K	1576 K
Location of max temperature	0.48	0.5
Location of max soot vol fraction	0.5	0.71

There has not been any experiment case study on ethylene-air crossflow for diffusional combustion. This study tends to analyze the crossflow case study using the coflow model and analyzing the trends in variation in velocity ratios.

RESEARCH CONTRIBUTION

For the first time, this research study contributes to the numerical analysis performed on crossflow diffusional combustion on ethylene-air streams. It also validates the soot, turbulent and radiation model that best predicts coflow diffusional combustion and comparing it to a similar experimental result.

In this study, the effect of velocity ratio on crossflow diffusion combustion is systematically investigated by numerical method. Its effect on mixing, temperature prediction, and soot production was analyzed. The RANS turbulent model, SST, and one-step soot model, with Rosseland radiation model, is used for the cross-flow analysis at various velocity ratios. It is found that inadequate mixing of fuel and air stream lead to an increase in temperature and soot volume fraction of crossflow jet as compared to its coflow jet flame. It is also found that increasing the velocity of the jet in crossflow (fuel), will increase temperature, as result of increase in heat released in reaction zone, and will lead to significant increase in soot production.

CHAPTER 5: CONCLUSION AND FUTURE WORK.

This section provides thesis conclusions and suggested future work. The results obtained are summarized as follows:

- The coflow diffusional combustion was best predicted using RANS SST turbulent model, one-step soot model and Rosseland radiation model with gravity. Results were compared and validated using experimental results from Coppalle & Joyeux and also proved Santu model was accurate.

- For the crossflow, increase in velocity of fuel jet increased temperature and soot volume fraction.

- The crossflow study also showed that as the fuel jet velocity/concentration increases, its maximum temperature and soot volume fraction, get further away from the proximity of jet inlet.

- The crossflow jet, when compared to the coflow jet of similar velocity ratio, the crossflow has higher temperature and soot production. This may be as a result of an inadequate mixing of fuel and air streams in crossflow jet, as compared to the coflow jet.

- The coflow maximum temperature and soot are further away from the inlet proximity as compared to the crossflow. Due to an adequate mixing of fuel and air streams in the coflow jets.

Future work suggested for this study;

- For the coflow jet, it was observed Moss&Brookes with Lee oxidation model has a good soot production prediction, more work could be done by testing various

turbulent and radiation model outside the scope of this case study such as the discrete ordinate method.

- Performing experiments on crossflow to validate numerical data or analysis.

- Testing various turbulent, soot and radiation models to predict the best numerical model for crossflow jet, and validating results from trusted sources or from experimental results.

- Improving on better and consistent methods of obtaining data from crossflow combustion at various flame front. Unlike the coflow data which was easily generated for all cases at the center of the jet flame.

REFERNCES

1. H. Wang, M. Frenklach, A detailed kinetic modeling study of aromatics formation in laminar premixed acetylene and ethylene ames, Combustion and Flame 110 (12) (1997) 173-221.

2. G. Blanquart, P. Pepiot-Desjardins, H. Pitsch, Chemical mechanism for high temperature combustion of engine relevant fuels with emphasis on soot precursors, Combustion and Flame 156 (3) (2009) 588-607.

3. Thierry Poinsot, Denis Veynante, Theoritical and Numerical Combustion, R.T.Edwards, Inc, 2005, 2nd Edition, ISBN 1-930217-10-2.

4. Williams, F. A. 1985 Combustion theory, Benjamin Cummings, Menlo Park, CA.

5. Kuo, K. K. 1986 Principles of Combustion, John Wiley, New York.

6. J. Warnatz, U. Mass, and R.W. Dibble. Combustion: Physical and Chemical Fundamentals, Modeling and Simulaiton, Experiments, Pollutant Formation. Springer-Verlag, Berlin Heidelberg, third edition, 2001.

7. S.B. Pope. Computationally efficient implementation of combustion chemistry using in situ adaptive tabulation. Combust. Theory & Modelling, 1(1):41-63, March 1997.

8. L. Muniz & M. G. Mungal, Heat Release and Buoyancy on Flow Structure and Entrainment in Turbulent Non-premixed Flames, Combustion and Flame, 126, 2001, 1402-1420.

9. https://en.wikipedia.org/wiki/File:Jet_engine.svg

10. Wilcox, David C (1998). "Turbulence Modeling for CFD". Second edition. Anaheim: DCW Industries, 1998. pp. 174.

11. Launder, B. E., and Sharma, B. I. (1974), "Application of the Energy Dissipation Model of Turbulence to the Calculation of Flow Near a Spinning Disc", Letters in Heat and Mass Transfer, vol. 1, no. 2, pp. 131-138.

12. Henk Kaarle Versteeg, Weeratunge Malalasekera (2007). An Introduction to Computational Fluid Dynamics: The Finite Volume Method. Pearson Education Limited. ISBN 9780131274983.

13. Wilcox, D.C. (1988), "Re-assessment of the scale-determining equation for advanced turbulence models", AIAA Journal, vol. 26, no. 11, pp. 1299-1310.

14. Wilcox, D.C. (2004), Turbulence Modeling for CFD, ISBN 1-928729-10-X, 2nd Ed., DCW Industries, Inc.

15. Menter, F. R. (1993), "Zonal Two Equation k-ω Turbulence Models for Aerodynamic Flows", AIAA Paper 93-2906.

16. Menter, F. R. (1994), "Two-Equation Eddy-Viscosity Turbulence Models for Engineering Applications", AIAA Journal, vol. 32, no 8. pp. 1598-1605.

17. G.M. Faeth and U. O. Koylu. Soot morphology and optical properties in non-premixed turbulent flame environment. Combust. Sci. and Tech., 108:207-229, 1995.

18. M.F. Modest. Radiative Heat Transfer. Academic Press, second edition, 2003.

19. M.Y. Choi, G.W. Mulholland, A. Hamins, and T. Kashiwagi. Comparisons of the soot volume fraction using gravimetric and light extinction techniques. Combust. Flame, 102:161{169, 1995.

20. G. Ma , J. Z. Wen , M. F. Lightstone & M. J. Thomson (2005) Optimization Of Soot Modeling In Turbulent Nonpremixed Ethylene/ Air Jet Flames, Combustion Science And Technology, 177:8, 1567-1602, Doi: 10.1080/00102200590956786.

21. Brookes, S.J. and Moss, J.B. (1999) Predictions of soot and thermal radiation properties in confined turbulent jet diffusion flames. Combust. Flame, 116, 486–503.

22. Wen, Z., Yun, S., Thomson, M.J., and Lightstone, M.F. (2003) Modeling soot formation in turbulent kerosene=air jet diffusion flame. Combust. Flame, 135, 323–340.

23. Hall, R.J., Smooke, M.D., and Colket, M.B. (1997), Predictions of soot dynamics in opposed jet diffusion flames. In Dryer, F.L. and Sawyer, R.F. (Eds.) Physical and Chemical Aspects of Combustion: A Tribute to Irvine Glassman. Gordon & Breach Science Publishers, New York, 189–229.

24. Prado, G.P., Jagoda, J., Neoh, K., and Lahaye, J. (1981) A study of soot formation in premixed propane=oxygen flames by in-situ optical techniques and sampling probes. Proc. Combust. Instit., 18, 1127–1136.

25. Neoh, K.G., Howard, J.B., and Sarofim, A.F. (1980) Soot oxidation in flames. In Siegla, D.C. and Smith, B.W. (Eds.) Particulate Carbon, Plenum, New York.

26. M. Khan and G. Greeves. "A Method for Calculating the Formation and Combustion of Soot in Diesel Engines". In N. H.Afgan and J. M.Beer, editors Heat Transfer in Flames. Chapter 25 Scripta, Washington DC. 1974.

27. P. A. Tesner, T. D. Snegiriova, and V. G. Knorre. "Kinetics of Dispersed Carbon Formation". Combustion and Flame. 17. 253–260. 1971.

28. Seaid, M., Klar, A. & Pinnau, R., Numerical solvers for radiation and conduction in high temperature gas flows. Journal of Flow Turbulence and Combustion, **75**(1), pp. 173–190, 2005. http://dx.doi.org/10.1007/s10494-005-8589-y

29. Crnjac, Peter & Škerget, L & Ravnik, Jure & Hriberšek, Matjaz. (2017). Implementation of the Rosseland and the P1 Radiation Models in the System of Navier-Stokes Equations with the Boundary Element Method, International Journal of Computational Methods and Experimental Measurements. 5. 348-358. 10.2495/CMEM-V5-N3-348-358.

30. R. Siegel and J. R. Howell. Thermal Radiation Heat Transfer. Hemisphere Publishing Corporation, Washington DC, 1992.

31. ANSYS CFX-Solver: Theory Guide, 1996-2006 ANSYS Europe, Ltd., ANSYS CFX Release 11.0, 2006.

32. https://www.sharcnet.ca/Software/Fluent6/html/ug/node577.htm

33. David O. Lignell, Jacqueline H. Chen, Philip J. Smith, Three dimensional direct numerical simulation of soot formation and transport in a temporally evolving nonpremixed ethylene jet flame, Combustion and Flame 155 (2008) 316–333

34. John C. Hewson1, David O. Lignell, Sean P. Kearney, Daniel R. Guildenbecher, Victoria Lansinger, One-dimensional turbulence simulation of soot and enthalpy evolution in ethylene jet diffusion flames, SAND2015-1740C.

35. S. P. Kearney and D. J. Scoglietti. Opt. Lett., 38 (2013) 833–835.

36. Krishna C. Kalvakala. Viswanath R. Katta, Suresh K. Aggararwal, Effects of oxygen-enrichment and fuel unsaturation on soot and NOx emissions in ethylene, propane and propene flames, Combustion and Flame 187 (2018) 217-229.

37. J.Y.Hwang and S.H.Chung, Growth of soot paticles in counterflow diffusion flames of ethylene, Combustion and flame 125:752-762 (2001).

38. Lorenzo Mazzei, Stefano Puggelli, Davide Bertini, Daniele Pampaloni, Antonio Andreini, Modelling soot production and thermal radiation for turbulent diffusion flames, Energy Procedia 126 (201709) 826-833.

39. Young K, Stewart C, Moss J. Soot Formation in Turbulent Nonpremixed Kerosine-Air Flames Burning at Elevated Pressure: Experimental Measurement. Twenty-Seventh Symp Int Combust Combust Inst 1994:609–17

40. Smooke, M.D., McEnally, C.S., Pfefferle, L.D., Hall, R.J., and Colket, M.B. (1999) Computational and experimental study of soot formation in a coflow, laminar diffusion flame. Combust. Flame, 117, 117–139.

41. Gopalendu Pal, Ankur Gupta, Michael F. Modest, Daniel C. Haworth, Comparison of accuracy and computational expense of radiation models in simulation of non-premixed turbulent jet flames, Combustion and Flame 162 (2015) 2487–2495.

42. L.Wang, D. Haworth, S. Turns, M. Modest, Interactions among, thermal radiation, and NOx emissions in oxygen–enriched turbulent non–premixed flames: a computational fluid dynamics modeling study, Comb. flame, 141 (2005) 170–179

43. L.Wang, M.F.Modest, D. C. Haworth and S. R. Turns, Modeling nongrey gas-phase and soot radiation in luminous turbulent nonpremixed jet flames. Comb. Theory and Modeling, (2005) vol. 9 No. 3 479-498.

44. Young, K.J. and Moss, J.B. (1995) Modeling sooting turbulent jet flames using an extended flamelet technique. Combust. Sci. Technol., 105, 33–53.

45. D.O. Lignell, J.H. Chen, P.J. Smith, T. Lu, C.K. Law, two-dimensional decaying turbulence simulations have shown the importance of multidimensional flame dynamical effects on soot concentration, Combust. Flame 151 (1–2) (2007) 2–28.

46. J. Doom, J. Oefelein, Simulation of an ethylene-air jet flame with soot and radiation modeling, Preprint submitted to Combustion and Flame, May, 2010.

47. K. M. Leung, R. P. Lindstedt, W. P. Jones. A simplified reaction mechanism for soot formation in nonpremixed flames, Combust. Flame. 87 (1991), 289-305.

48. J. Appel, H. Bockhorn, M. Frenklach, Kinetic modeling of soot formation with detailed chemistry and physics: laminar premixed flames of C2 hydrocarbons. Combust. and Flame 121, (2000), 122–136.

49. H. Wang, D.X. Du, C.J. Sung, C.K. Law, Experiments and numerical simulation on soot formation in opposed–jet ethylene diffusion flames. 26th Sym (Int) Comb. Inst. (1996), 2359–2368.

50. A. Coppalle, D. Joyeux, Temperature and soot volume fraction in turbulent diffusion flames measurements of mean and fluctuating values. Combustion and Flame. 96, 275-285, 1994.

51. Santu Golder and Jeffery Doom, Simulation of an ethylene flame with turbulence, soot and radiation modeling, 55th AIAA Aerospace Sciences Meeting, AIAA 2017-0540.

52. J. Doom, Simulation using flamelet radiation modeling. 54th AIAA Aerospace Sciences Meeting.

53. D. Carbonell, C. Perez-Segarra, P.J. Coelho, A. Oliva, Flamelet mathematical models for non-premxied laminar combustion. Combust and Flame 156, 334 - 347, 2009.

54. Liangyu Wang, Detailed Chemistry, soot and radiation calculations in turbulent reacting flows, A Thesis in Mech Engrg Pennsylvania state university, 2004.

55. D. McCubbin, Health Impacts of Diesel, Based on Data from the National Scale Air Toxics Assessment, http: //www.catf.us/publications/reports/200910-NATA Diesel 2002 Health impacts.pdf, Oct 2009.

56. S.M. Correa. Power generation and aeropropulsion gas turbines: from combustion science to combustion technology. Proc. Combust. Institute, 27:1793-1870, 1998.

57. D. Veynante and L. Vervisch. Turbulent combustion modeling. Prog. Energy Combust. Sci., 28:193-266, 2002.

58. Pitsch, H. & Peters, N. 1998 Unsteady flamelet modeling of turbulent hydrogen-air diffusion flames. 27th Symp. (Int.) on Combustion, The Combustion Institute, Pittsburgh, 1057-1064.

59. Pitsch, H. & Peters, N. 1998 A consistent flamelet formulation for non-premixed combustion considering differential diffusion effects. Combust. Flame 114, 26-40.

60. Peters, N. 2000 Turbulent combustion, Cambridge University Press

61. C. P. Fenimore and G. W. Jones. "Oxidation of soot by hydroxyl radicals". J. Phys. Chem. 71. 593–597. 1967.

62. Z. Wen, S. Yun, M. J. Thomson, and M. F. Lightstone. "Modeling Soot Formation in Turbulent Kerosene/Air Jet Diffusion Flames". Combustion and Flame. 135. 323–340. 2003.

63. R. J. Hall, M. D. Smooke, and M. B. Colket. Physical and Chemical Aspects of Combustion. Gordon and Breach. 1997.

64. K. B. Lee, M. W. Thring, and J. M. Beer. Combustion and Flame. 6. 137–145. 1962.

APPENDIX A

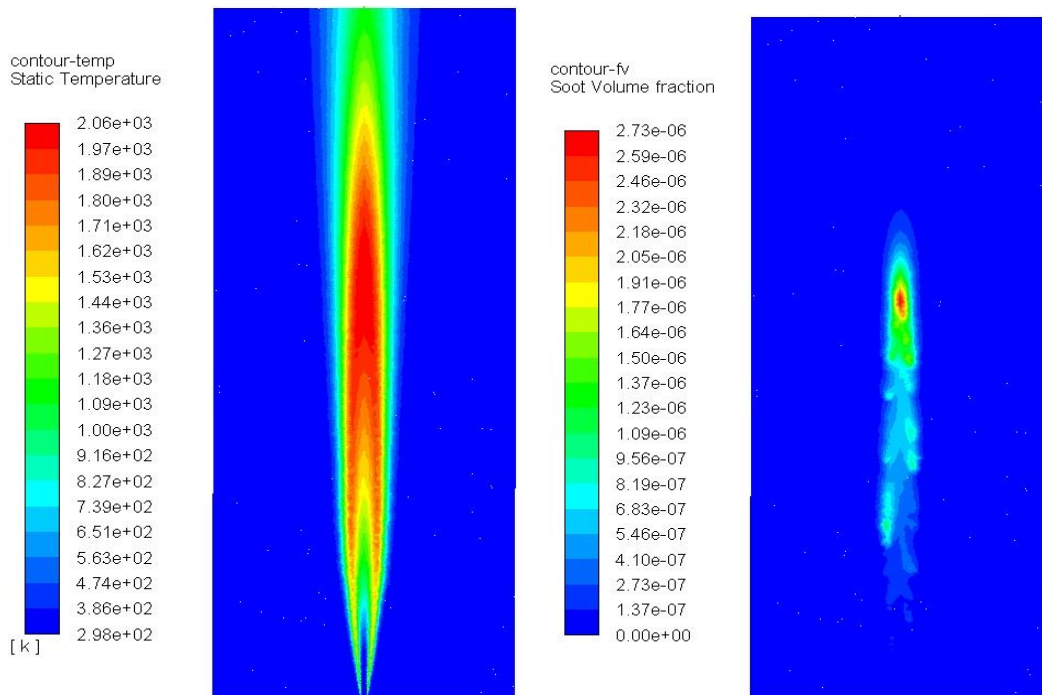Images for coflow data at various RANS turbulent, soot and radiation model, in the presence or absence of gravity.
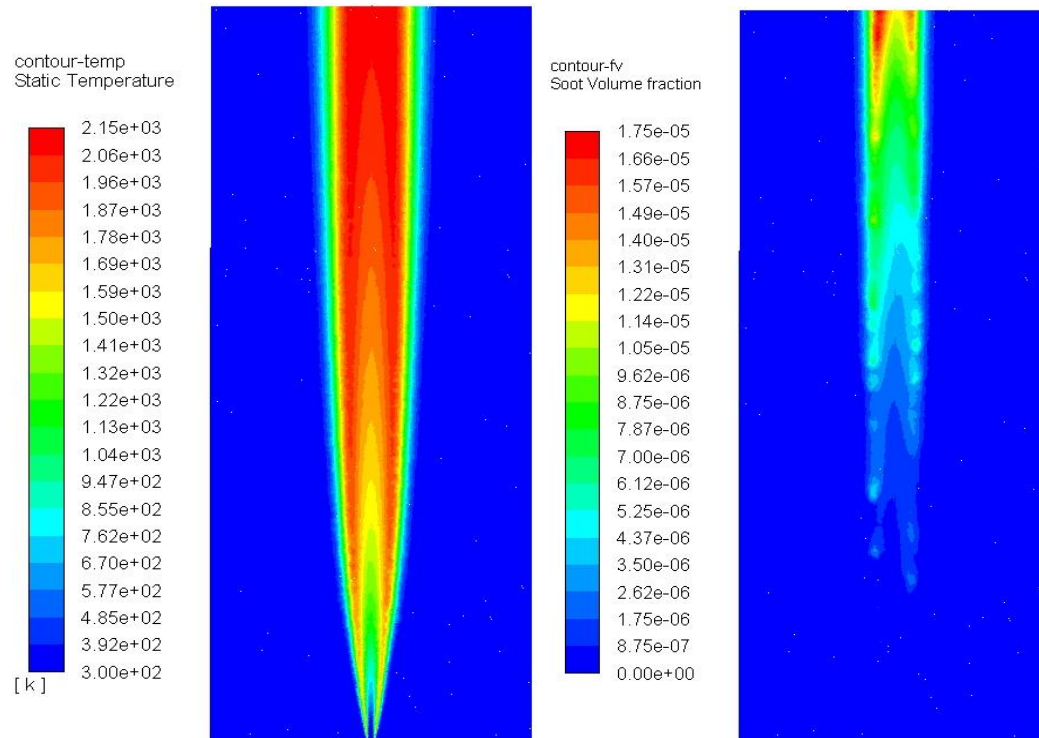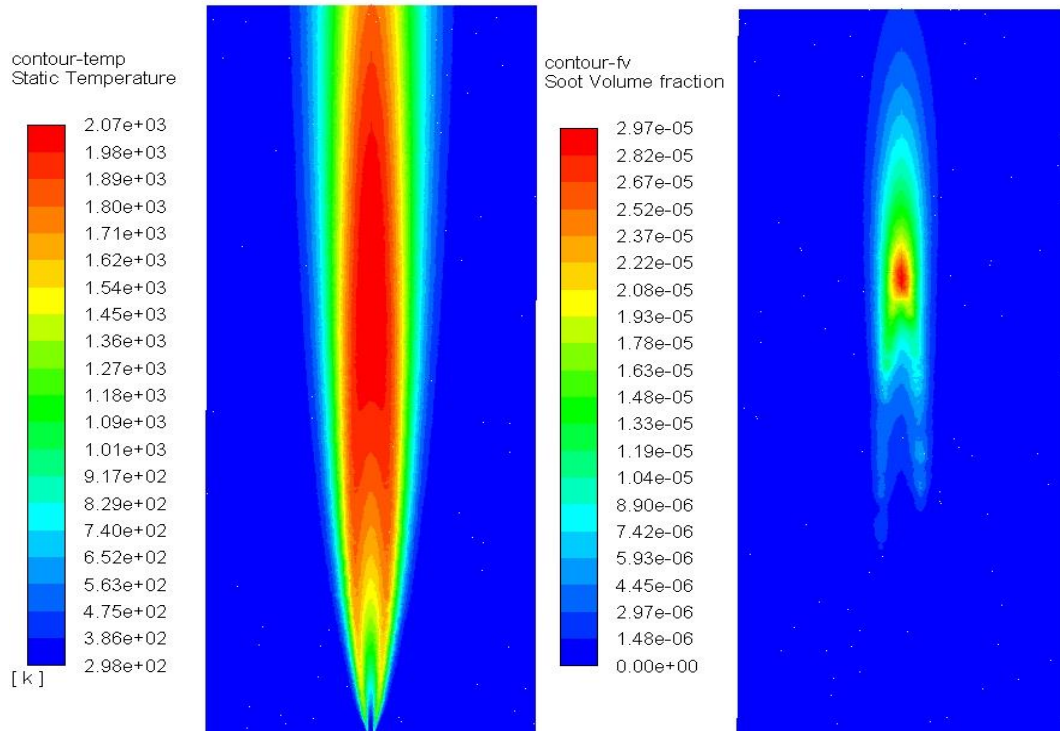

Figure 33 : Temperature & soot volume fraction for one -step_ke_No radiation_No gravity model.
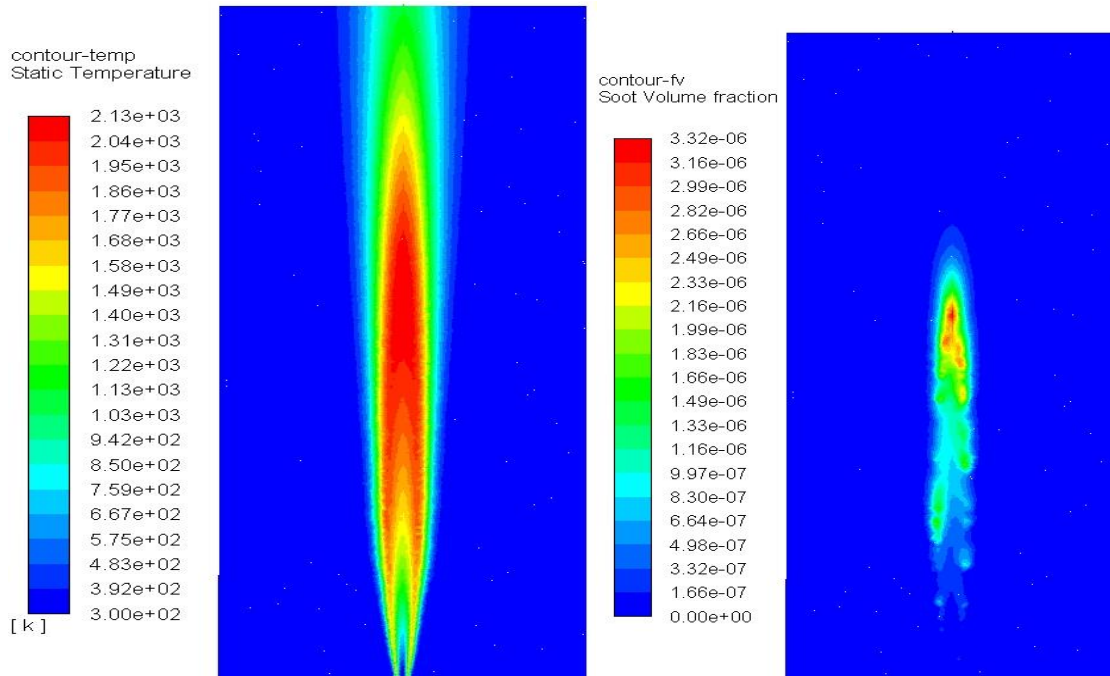
Figure 34: Temperature & soot volume fraction for one step_k-epsilon_P1 radiation_

with gravity

Figure 35: Temperature & soot volume fraction for one step_k-epsilon_Rosseland

radiation with gravity.
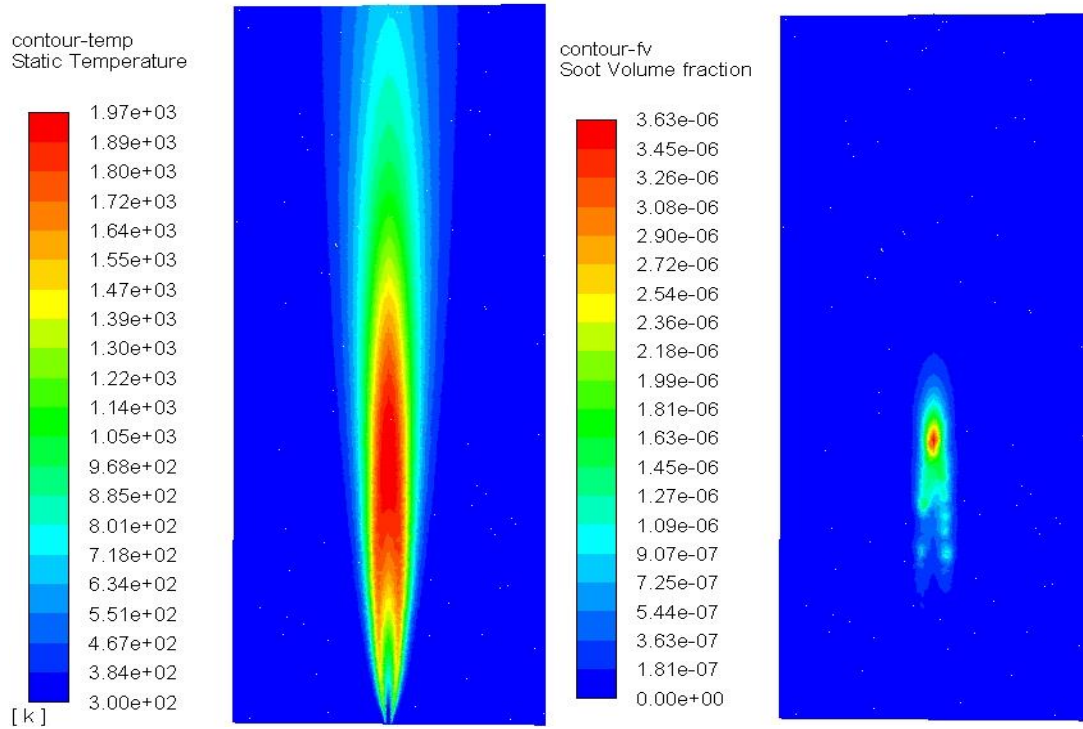
Figure 36: Temperature & soot volume fraction for one steo_k-omega_P1 with gravity
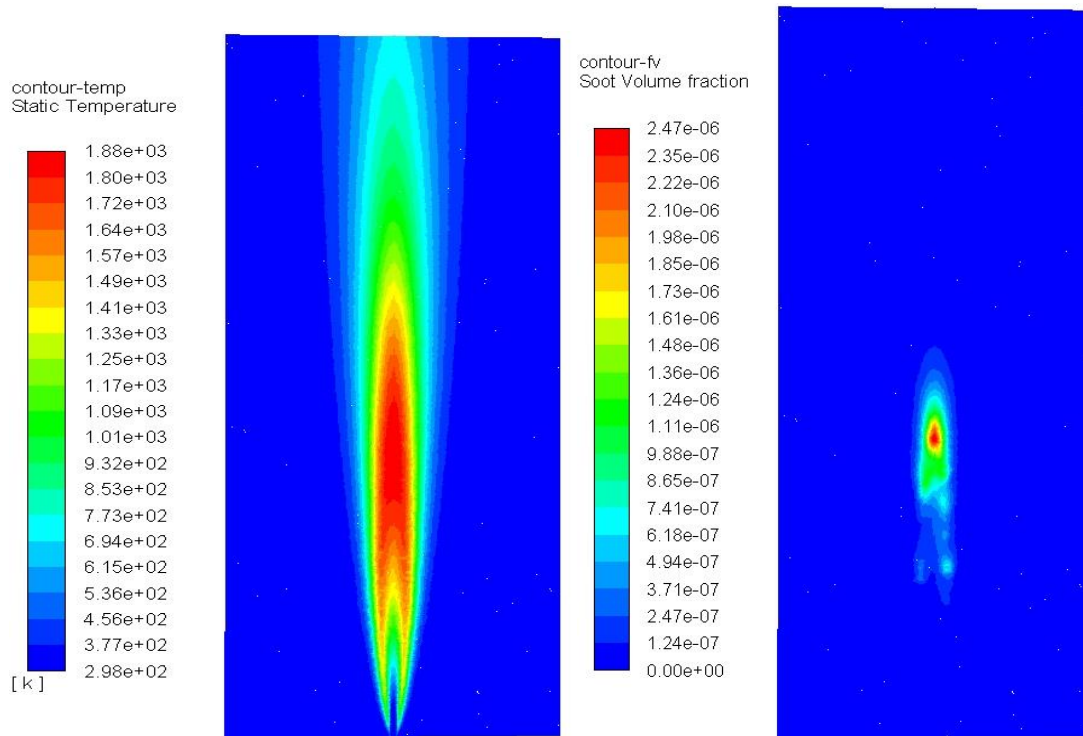
Figure 37: Temperature & soot volume fraction for one step_k-omega_Rosseland_gravity

Figure 38: Temperature & soot vol. fraction for one step_SST_No radiation_ No gravity
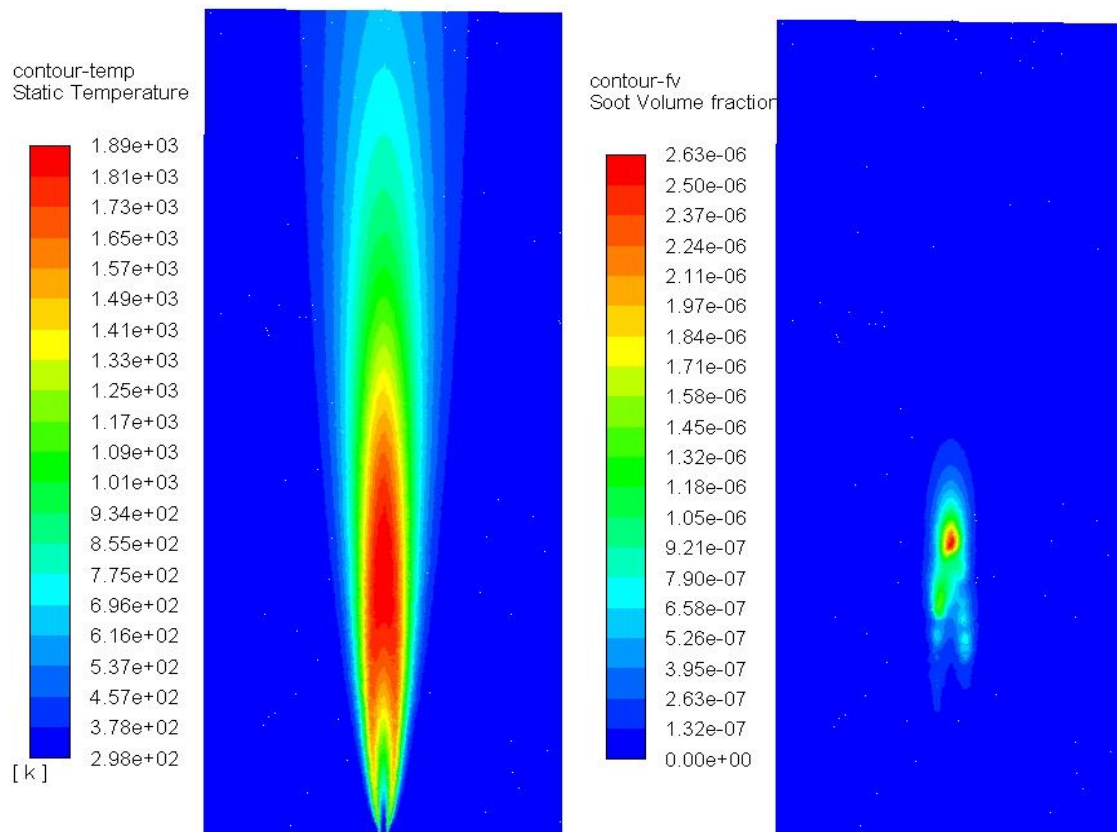
Figure 39: Temperature & soot vol. fraction for one step_SST_P1 with gravity.
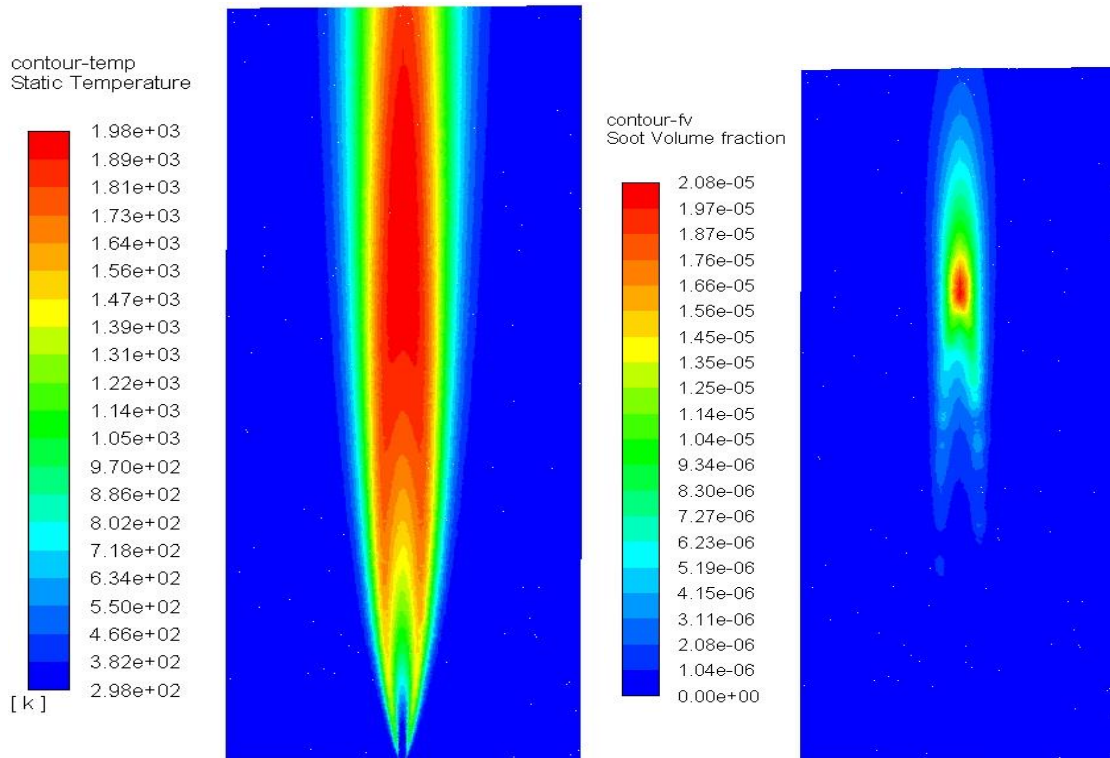
Figure 40: Temperature & soot vol. fraction for one step_SST_Rosseland_ No gravity
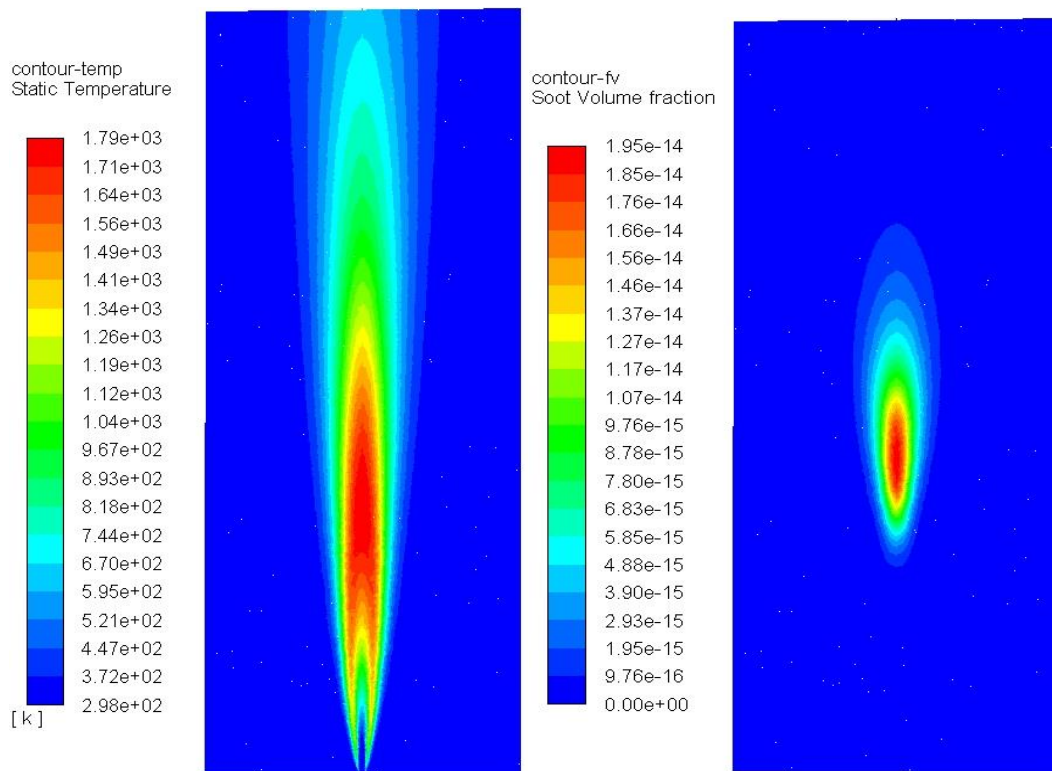
Figure 41: Temperature & soot vol. fraction for two step_ SST_Rosseland with gravity.
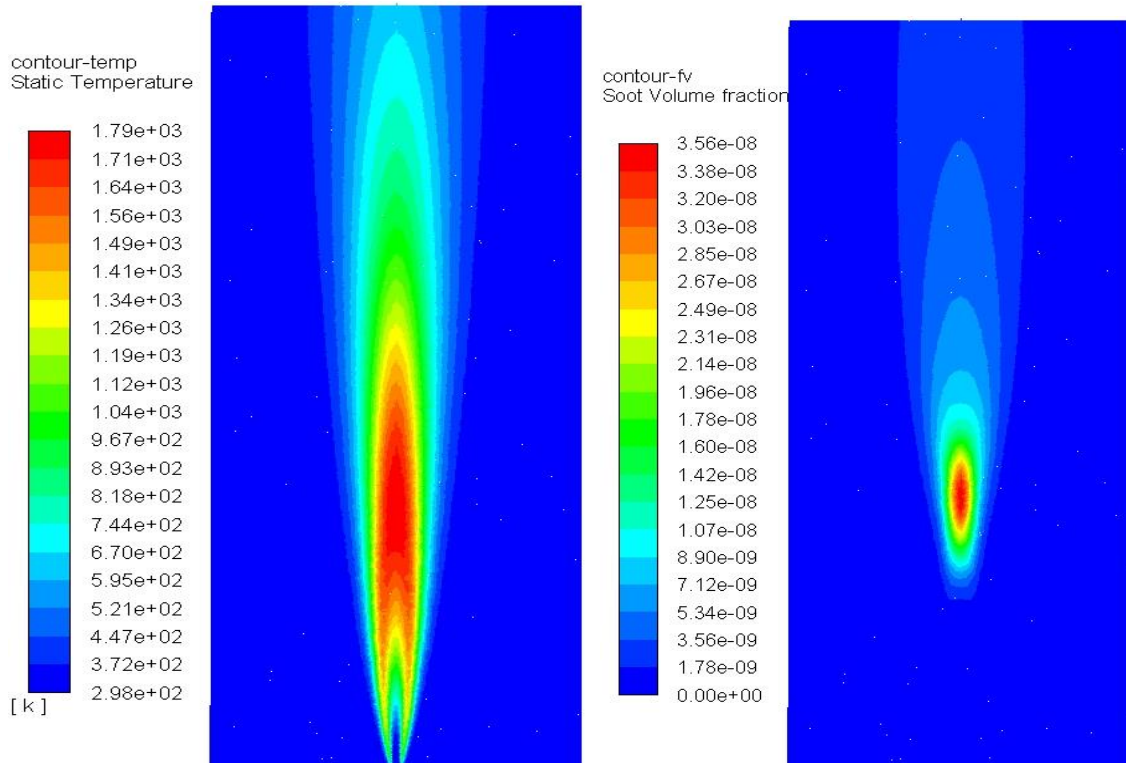
Figure 42: Temperature & soot vol. fraction for Moss & Brookes with Fenimore jones oxidation model_SST_Rosseland model with gravity
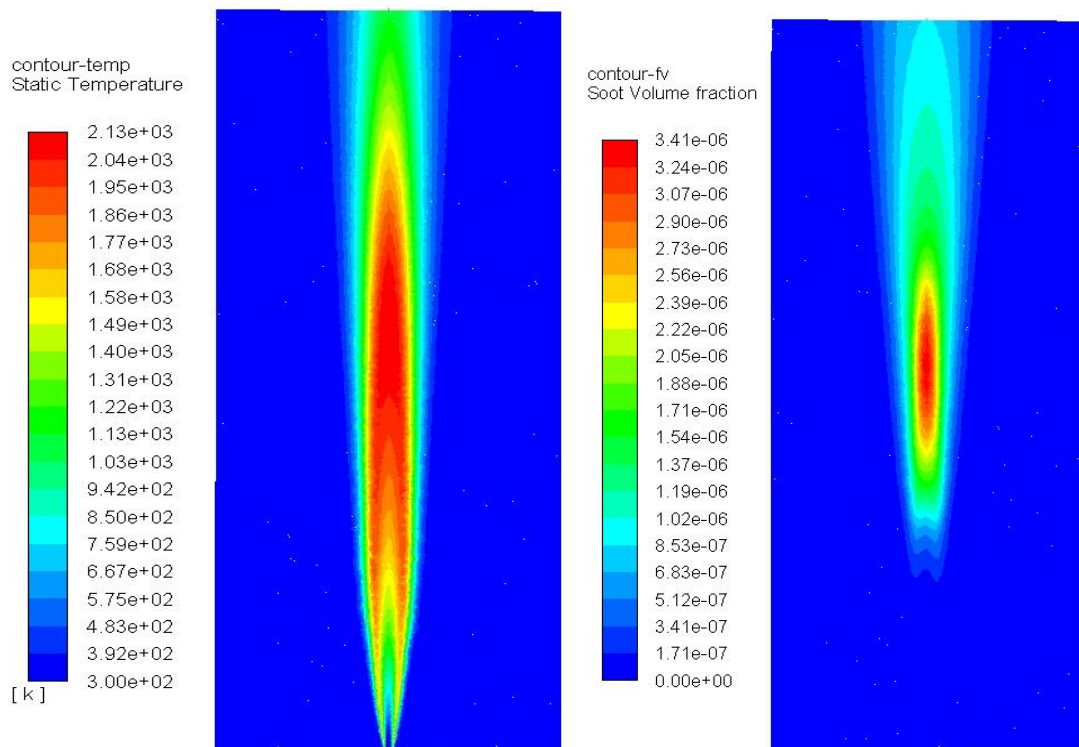
Figure 43: Temperature & soot vol. fraction for Moss & Brookes with Lee oxidattion _k-epsilon_P1 radiation with gravity.
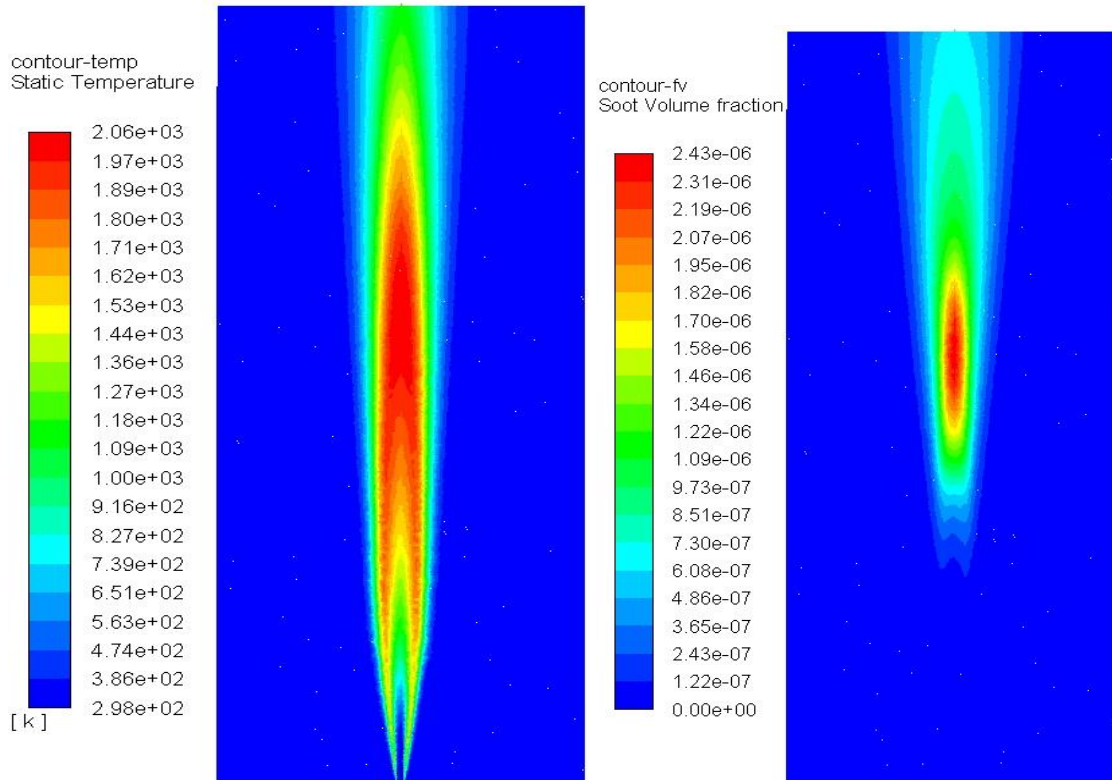
Figure 44: Temperature & soot vol. fraction for Moss & Brookes with Lee oxidattion _k-epsilon_Rosseland radiation with gravity.
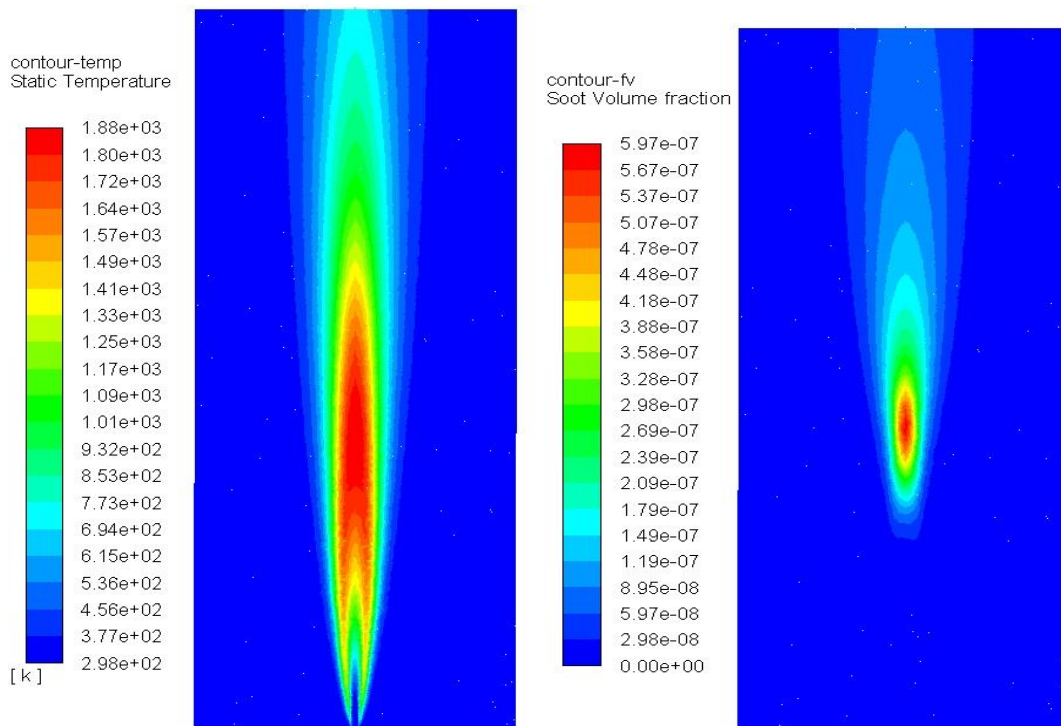

Figure 45: Temperature & soot vol. fraction for Moss & Brookes with Lee oxidattion _k-omega_Rosseland radiation with gravity.
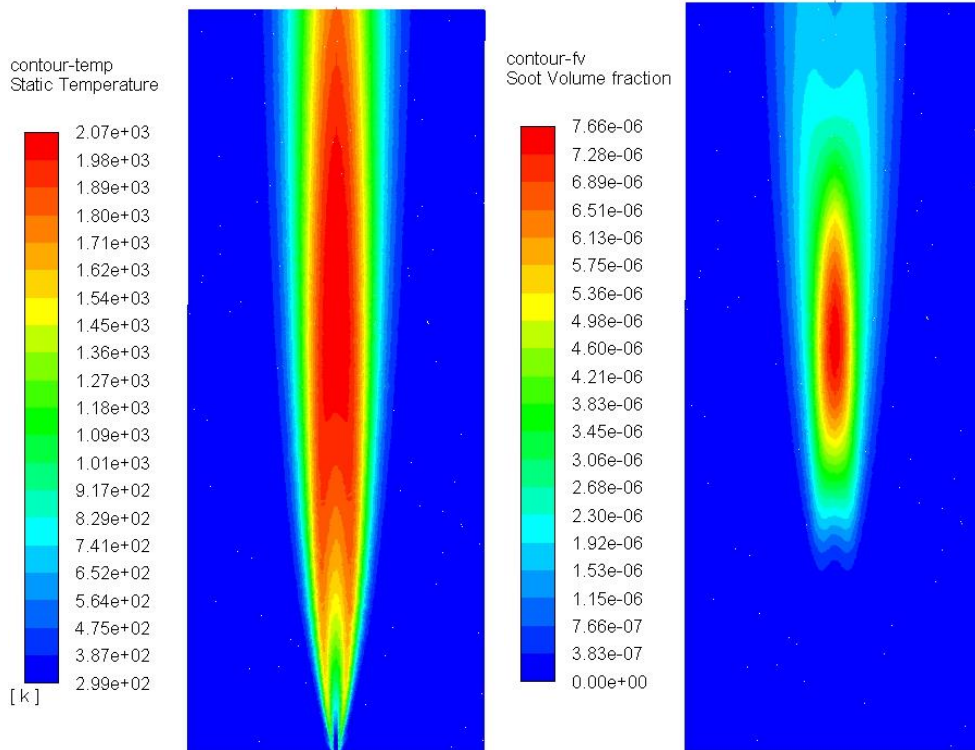
Figure 46: Temperature & soot vol. fraction for Moss & Brookes with Lee oxidation _SST_No radiation in absence of gravity.
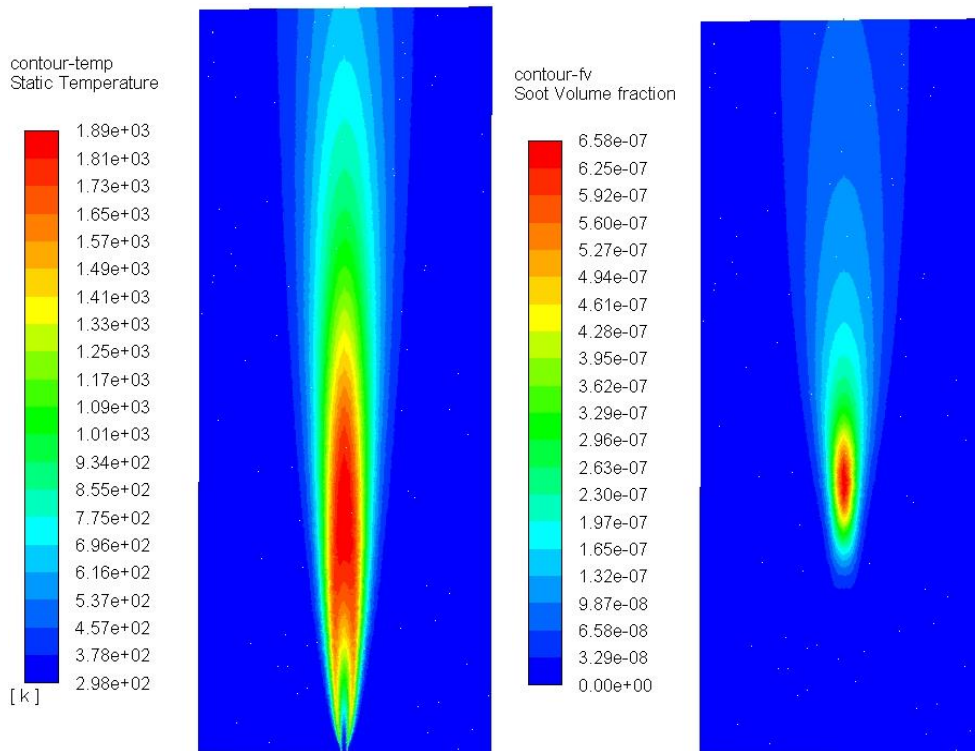

Figure 47: Temperature & soot vol. fraction for Moss & Brookes with Lee oxidation_SST _P1 radiation with gravity.
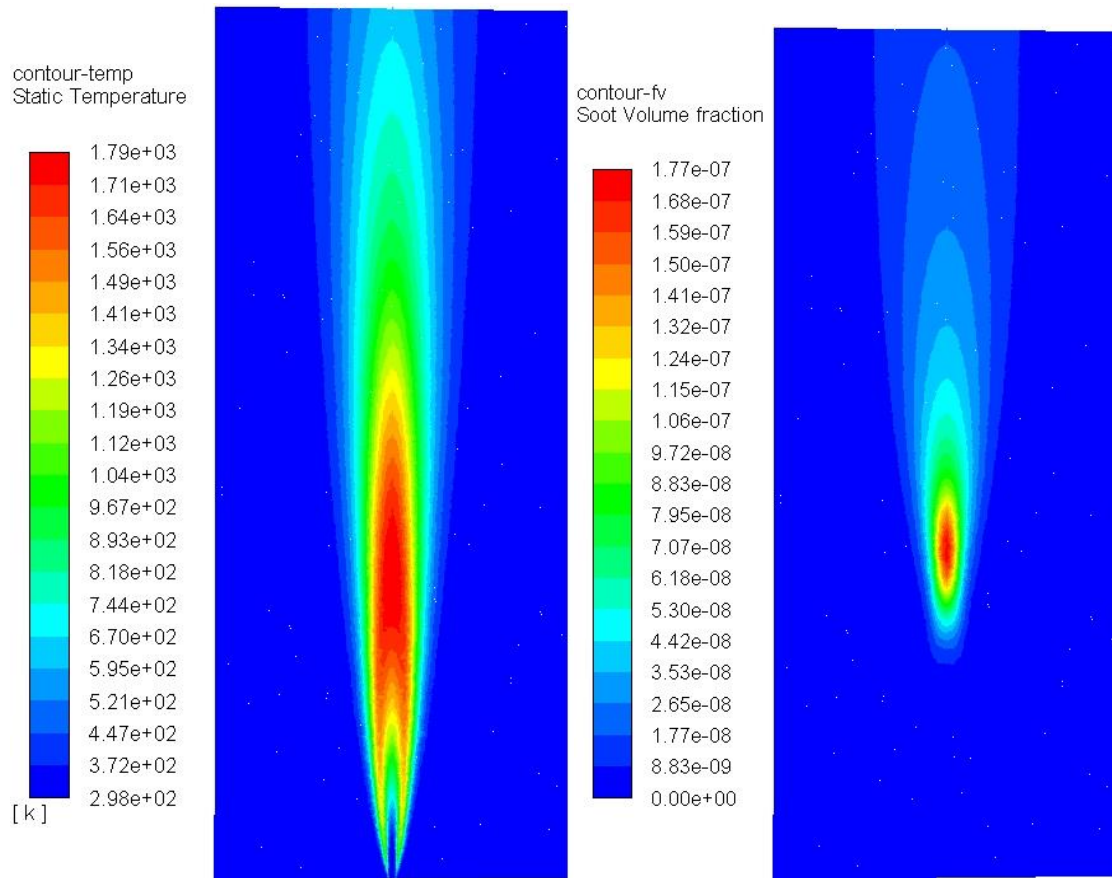
Figure 48: Temperature & soot vol. fraction for Moss & Brookes with Lee oxidation

_SST _ Rosseland radiation with gravity